Groundwater Level Prediction Using a Multiple Objective Genetic Algorithm-Grey Relational Analysis Based Weighted Ensemble of ANFIS Models

Dilip Kumar Roy [1,*], Sujit Kumar Biswas [1], Mohamed A. Mattar [2,3,4], Ahmed A. El-Shafei [2,4,5], Khandakar Faisal Ibn Murad [1], Kowshik Kumar Saha [6,7], Bithin Datta [8] and Ahmed Z. Dewidar [4,*]

[1] Irrigation and Water Management Division, Bangladesh Agricultural Research Institute, Gazipur 1701, Bangladesh; sujitbari@yahoo.com (S.K.B.); faisal.ae.bau@gmail.com (K.F.I.M.)
[2] Department of Agricultural Engineering, College of Food and Agriculture Sciences, King Saud University, Riyadh 11451, Saudi Arabia; mmattar@ksu.edu.sa (M.A.M.); aelshafei1bn.c@ksu.edu.sa (A.A.E.-S.)
[3] Agricultural Research Centre, Agricultural Engineering Research Institute (AEnRI), Giza 12618, Egypt
[4] Prince Sultan Institute for Environmental, Water and Desert Research, King Saud University, P.O. Box 2454, Riyadh 11451, Saudi Arabia
[5] Department of Agricultural Engineering, Faculty of Agriculture (El-Shatby), Alexandria University, Alexandria 21545, Egypt
[6] Faculty V, Technische Universität Berlin, Straße des 17. Juni 135, 10623 Berlin, Germany; kksaha.bari@gmail.com
[7] ASICT Division, Bangladesh Agricultural Research Institute, Gazipur 1701, Bangladesh
[8] Discipline of Civil Engineering, College of Science and Engineering, James Cook University, Townsville, QLD 4811, Australia; bithin.datta@jcu.edu.au
* Correspondence: dilip.roy@my.jcu.edu.au (D.K.R.); adewidar@ksu.edu.sa (A.Z.D.)

Abstract: Predicting groundwater levels is critical for ensuring sustainable use of an aquifer's limited groundwater reserves and developing a useful groundwater abstraction management strategy. The purpose of this study was to assess the predictive accuracy and estimation capability of various models based on the Adaptive Neuro Fuzzy Inference System (ANFIS). These models included Differential Evolution-ANFIS (DE-ANFIS), Particle Swarm Optimization-ANFIS (PSO-ANFIS), and traditional Hybrid Algorithm tuned ANFIS (HA-ANFIS) for the one- and multi-week forward forecast of groundwater levels at three observation wells. Model-independent partial autocorrelation functions followed by frequentist lasso regression-based feature selection approaches were used to recognize appropriate input variables for the prediction models. The performances of the ANFIS models were evaluated using various statistical performance evaluation indexes. The results revealed that the optimized ANFIS models performed equally well in predicting one-week-ahead groundwater levels at the observation wells when a set of various performance evaluation indexes were used. For improving prediction accuracy, a weighted-average ensemble of ANFIS models was proposed, in which weights for the individual ANFIS models were calculated using a Multiple Objective Genetic Algorithm (MOGA). The MOGA accounts for a set of benefits (higher values indicate better model performance) and cost (smaller values indicate better model performance) performance indexes calculated on the test dataset. Grey relational analysis was used to select the best solution from a set of feasible solutions produced by a MOGA. A MOGA-based individual model ranking revealed the superiority of DE-ANFIS (weight = 0.827), HA-ANFIS (weight = 0.524), and HA-ANFIS (weight = 0.697) at observation wells GT8194046, GT8194048, and GT8194049, respectively. Shannon's entropy-based decision theory was utilized to rank the ensemble and individual ANFIS models using a set of performance indexes. The ranking result indicated that the ensemble model outperformed all individual models at all observation wells (ranking value = 0.987, 0.985, and 0.995 at observation wells GT8194046, GT8194048, and GT8194049, respectively). The worst performers were PSO-ANFIS (ranking value = 0.845), PSO-ANFIS (ranking value = 0.819), and DE-ANFIS (ranking value = 0.900) at observation wells GT8194046, GT8194048, and GT8194049, respectively. The generalization capability of the proposed ensemble modelling approach was evaluated for forecasting 2-, 4-, 6-, and 8-weeks ahead groundwater levels using data from GT8194046. The evaluation results confirmed the useability of the ensemble modelling for forecasting groundwater

levels at higher forecasting horizons. The study demonstrated that the ensemble approach may be successfully used to predict multi-week-ahead groundwater levels, utilizing previous lagged groundwater levels as inputs.

1. Introduction

Groundwater aquifers are considered as vital sources of the world's potable water supplies and take part in an essential role in the sustainability of irrigated agriculture; domestic and industrial water supplies in areas where good quality surface water is inadequate. Human pressure due to population growth, increasing water demand to different sectors, and a changing climate have created an enhanced pressure on groundwater resources. As a consequence, groundwater systems are experiencing rapid degradation. Although human intervention, such as over-pumping, is considered as the prime indicator of groundwater level declination, climate change, as evidenced by recent projections, has indicated that the situation will become even worse earlier than was anticipated [1]. Excessive abstraction of groundwater resources leads to continuous depletion and variable fluctuations of groundwater level, causing a variety of problems such as lowering of the suction heads of pumps, reduction of crop yields due to inadequate irrigation water supplies, decrease in potable water supplies for domestic and industrial purposes, and degradation of water quality, among others. As with many areas in the world, groundwater is the most important usable form of water reserves in Bangladesh, where approximately 80% of the total population depends primarily on the groundwater reserves for their water needs [2]. Therefore, proper management and sustainable utilization of the scanty groundwater reserves in the aquifer in an efficient manner are imperative to secure continuous supplies of groundwater for future generations. Accurate prediction and forecasting of future groundwater level fluctuations may aid in developing such a meaningful groundwater management strategy.

Numerical simulation models of groundwater flow processes have traditionally been applied in groundwater hydrology to better understand the underlying system processes while predicting the future scenarios of groundwater levels [3–5]. However, predicting groundwater levels using these physically-based models require a detailed understanding of the aquifer properties, as well as expertise and in-depth knowledge of the modeler about the aquifer geometry and modelling techniques. It is often difficult to obtain relevant and good quality data on aquifer properties and other appropriate prerequisites, i.e., model "initial and boundary conditions" required to develop physically-based models. Sometimes, unavailable data are substituted by assumptions made on the data based on the prior knowledge of the modeler regarding the model domain. These assumptions and estimations may lead to difficulties in the calibration and validation processes, which are very important in employing the developed model for prediction purposes. To overcome these unavoidable complexities associated with physically-based numerical modelling approaches, data-driven prediction modelling approaches relying on machine-learning and artificial intelligence have been introduced and applied in hydrology [6–12]. Data-driven modelling does not require an explicit definition of the parameters of the physical systems being modelled. In data-driven modelling approaches, a direct mapping or correlation between the predictors (inputs) and responses (outputs) of a model is established by way of an iterative learning method of a machine-learning algorithm [13]. Artificial Neural Networks (ANN)-based data-driven prediction models have been found to perform as good as or even better than the physically-based simulation models in the field of prediction of nonlinear time series data, e.g., groundwater table data [14,15]. As such, there has been a growing appreciation that data-driven approaches can be utilized as an alternative

modelling approach for capturing nonlinear dynamics of the aquifer responses quite accurately [16–19].

Groundwater level prediction comes into play when it is an essential task to evaluate the dynamics of the groundwater system, i.e., how much groundwater is being abstracted from the aquifer system and how much is permitted to be abstracted. Adequately precise short- to medium-term groundwater level prediction aids in developing a sustainable and flexible management strategy in areas where climate change-induced droughts or human-induced over-pumping is a major driving force [20–22]. Thus, groundwater level prediction has been an interesting topic in the hydrological research area. Numerous data-driven modelling methods are being increasingly used since they require less data and are easier to apply than conventional hydrogeological modelling methodologies [23]. Several approaches have recently been utilized in the research domain of groundwater level predictions. These include machine learning-based prediction modelling [21,22,24], ANNs [25–27], hybridized wavelet transform—machine learning methods [16,28–30], hybridized ensemble empirical mode decomposition and machine learning-based models [31], nonlinear autoregressive with exogenous inputs (NARX) neural networks [21], ARIMA-particle swarm optimization [32], ANN—whale algorithm [33], integrated linear polynomial and nonlinear system identification models [34], ANFIS [30,35–38], wavelet—ANFIS [39], Support Vector Machine (SVM) [35,40], hybrid SVM-PSO [41], Gaussian Process Regression [30], Genetic Programming [42], Facebook's prophet approach of groundwater level forecasting [43], physics-inspired coupled space-time artificial neural networks [44]. A detailed review of artificial intelligence-based approaches to groundwater level modelling is given in [45]. It is obvious that a variety of modelling methodologies have been used to anticipate groundwater level fluctuations with differing degrees of prediction accuracies. It is also clear that recommending a specific prediction model for a specific problem, such as predicting groundwater level fluctuations, is difficult, if not impossible. Therefore, more advanced approaches to groundwater level prediction are necessary for increasing the prediction accuracy of groundwater level fluctuations.

A hybrid/coupled model or an ensemble of models is likely to perform better than an individual prediction model [45]. Different types of prediction models may be developed for groundwater level forecasting and the best-performing models may be selected to combine them into an ensemble to have an optimum model performance. However, it is often very difficult, if not impossible, to identify the best machine-learning algorithm-based prediction models. In such cases, one of the most effective strategies for providing sufficiently accurate predictions has been to integrate the predictions of known best prediction models. Such integration of prediction models is generally referred to as an ensemble [46]. Ensemble predictions are believed to be more robust than a standalone prediction model with respect to grabbing hold of the true relationships between the inputs and outputs of a given prediction problem through incorporating the best features of the participating prediction models. Ensemble approaches include boosting, bagging, ranking, voting, and stacking [47]. In groundwater level forecasting, [28] utilized a least-square boosting algorithm to integrate different wavelet-neural network models. The present study seeks to employ a Multiple Objective Genetic Algorithm (MOGA) for integrating the prediction power of the evolutionary algorithm tuned ANFIS models in the framework of an ensemble prediction to predict one- and multi-week ahead groundwater levels.

An ensemble of data-driven prediction models can be created utilizing a simple averaging approach [48,49], in which the prediction of the selected individual models is combined by simply averaging the individual outputs. On the other hand, an ensemble of individual models can be formed by assigning weights to individual models with reference to their prediction precision [46,50]. Among them, the weighted average ensemble approach has gained popularity as it assigns weights to single prediction models regarding their prediction precision. Specific weights to single prediction models may be assigned through the utilization of the concepts of entropy [51], set pair analysis [52], or Dempster–Shafer evidence theory [53,54]. Another approach of assigning weights to individual

models is the utilization of a population-based optimization algorithm such as Genetic Algorithm (GA) [55], which is employed to find out the optimum weights with respect to either minimizing a cost index (the lower, the better) or maximizing a benefit index (the higher, the better). GA has previously been applied to allocate specific weights to standalone models based on a single performance index, e.g., MAE or RMSE [56]. However, the utilization of a single performance index in determining the weights is often not a suitable choice due to the conflicting nature of performance indexes. For instance, a model will possibly be regarded as the top performer among other models when a specific performance evaluation index is considered. In contrast, a different model may well be found as the worthiest model when another performance index is considered. This conflicting characteristic demands the incorporation of a set of performance indexes in determining the weights assigned to different individual prediction models for developing an integrated prediction model. Previous studies have successfully utilized the concepts of entropy weight [57] and Dempster–Shafer's theory of evidence [58,59] for incorporating different performance indexes of many prediction models to compute individual model weights. In this study, a Multiple Objective GA (MOGA) [60] is utilized to develop a trade-off between the benefits (the larger the values, the better will be the model predictions) and the cost indexes (the smaller the values, the better will be the model predictions). The conflicting objective functions considered are to maximize the sum of benefit indexes and to minimize the sum of cost indexes. The variables are the associated weights of individual models. The MOGA provides numerous alternate feasible solutions rather than a single solution. The best solution from the set of feasible solutions is selected by applying the concept of Grey Relational Analysis. To the best of the author's understanding, this method of weight assignment in the weighted average ensemble technique has not been applied previously in predicting groundwater levels.

Although long-term groundwater level prediction is desirable in many applications, including the development of groundwater management plans, short-term predictions often provide valuable insights into groundwater level fluctuations to better understand the underlying physical phenomena of an aquifer [15,25,61,62]. However, since the one-step-ahead prediction is strongly conditioned by exogeneous variables containing the stochastic component, the generalization capability of the proposed model needs to be investigated for multi-step ahead prediction horizons. Because groundwater flow and levels typically do not vary significantly over a short period [63], the present study aims at proposing both short-term (one-week ahead) and medium-term (2–8-weeks ahead) groundwater level forecasts using novel approaches.

The key motivation and focus of this study are to (1) delve into the potential of optimized ANFIS models in predicting one- and multi-step ahead groundwater level in the selected observation wells; (2) develop an ensemble of evolutionary algorithm optimized ANFIS models through weights assigned by a MOGA by incorporating a set of different performance indexes; and (3) provide a ranking of the ensemble and the individual ANFIS models through Shannon's entropy. To the best of the authors' understanding, this is the first time an ensemble of optimized ANFIS models (weighted average ensemble for which a MOGA determines the associated weights) has been employed to forecast one-step (one-week) and multi-step (multiple weeks) forward groundwater level fluctuations.

2. Methodology

2.1. Study Area and the Data

The study area, located between 24.46–24.73° N latitudes and between 88.40–88.65° E longitudes, is under the Tanore Upazila of Rajshahi district in the division of Rajshahi, Bangladesh. It has an aerial extent of 295.40 km^2. A river named Shiba flows across the study area, which provides an inadequate amount of irrigation water for irrigating the major crops. Barind Tract constitutes a major portion (81.8%) of the geologic formation. In comparison, Old Gangetic Floodplain (3%) and Tista Floodplain (4.8%) cover only a small portion of the geology. The remaining 10.4% of the entire area is occupied by homestead

areas, ponds, wetlands, and rivers [64]. The land formation of Tanore Upazila is composed mainly of clay loam (46%), loam (35%), and clay (8%) [65]. Pumped groundwater appears to be the prime water resource for household usage and crop irrigation. Excessive abstraction of groundwater from the aquifer has been increasing every year, resulting in the gradual declination of groundwater levels. As the study area is categorized as a flood-free zone in Bangladesh due to its high elevation with respect to the mean sea level, monsoon rainfall is the only source of water that can be percolated to the water-bearing strata to recharge the groundwater. However, the study area's thick and sticky clay surface is not favourable for the natural recharge of groundwater into the aquifer. The combined interaction of the low recharge potential of the land formation, inadequate rainfall, and increased groundwater abstraction result in a decline in groundwater level in the Tanore Upazila of Rajshahi district (the study area).

Previous data on groundwater level fluctuations were used to model future scenarios of groundwater table fluctuations in the selected observation wells of the study area, especially to provide a one-step-ahead forecast of groundwater levels. For this, weekly historical data on groundwater level fluctuations with a period from January 1980 to September 2018 were collected from Bangladesh Water Development Board. Collected data at different observation wells were carefully checked and three observation wells, namely GT8194046, GT8194048, and GT8194049, were selected based on the criterion of the least number of missing entries. The observation well GT8194046 is positioned between 24.68° N latitude and 88.53° E longitude. The position of the observation well GT8194048 is between 24.57° N latitude and 88.55° E longitude, whereas the observation well GT8194049 is situated between 24.63° N latitude and 88.58° E longitude. The study area and the positions of the observation wells inside the study area are shown in Figure 1.

However, there were some missing values in the groundwater level datasets in the selected observation wells. The missing entries of weekly groundwater level data accounted for 0.55% (11 missing entries out of 2021), 0.64% (13 missing entries out of 2021), and 0.70% (14 missing entries out of 2021) for the observation wells GT8194046, GT8194048, and GT8194049, respectively. These missing entries were imputed using the "nearest-neighbour" approach to data imputation. Missing entries in an input column were replaced with equivalent entries from the nearest-neighbour column by computing the Euclidean distance among the "nearest-neighbour" columns [66]. Table 1 presents a few descriptive statistics of the datasets (after imputation of the missing entries) at the selected observation wells. Table 1 reveals that the mean values of groundwater level data ranged between 8.80 m (at GT8194049) and 11.62 m (at GT8194048), whereas the standard deviation values varied between 4.29 m (at GT8194049) and 4.41 m (at GT8194046). The data at all observation wells possessed a longer right tail than the left tail in their distribution, as evidenced by the positive (right) skewness values (Table 1). On the other hand, the datasets showed "light-tailed" distributions because the kurtosis values are negative at all observation wells.

Table 1. Measures of the statistical parameter values for the groundwater level data (m) at the observation wells.

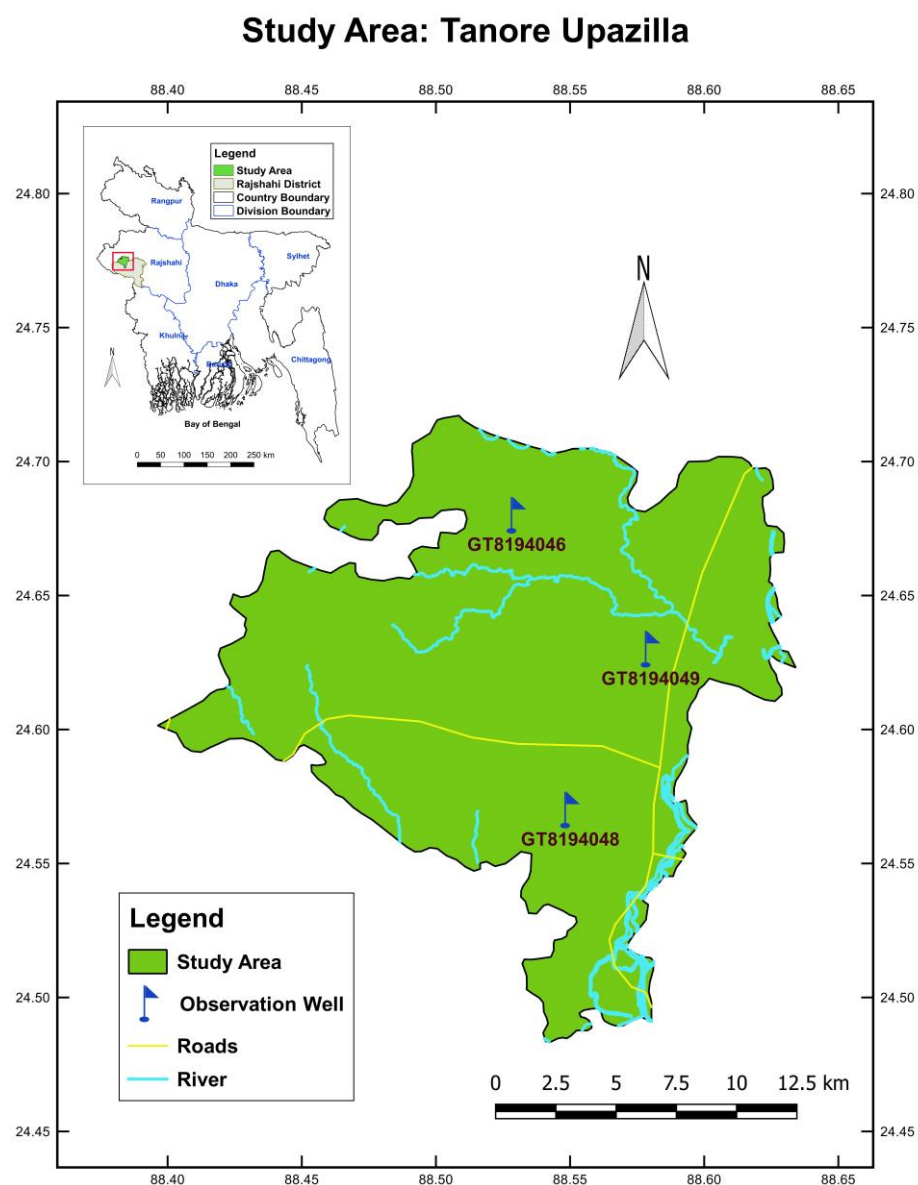| Obs. Wells	Min	Max	Mean	Median	STD	Skewness	Kurtosis
GT8194046	0.91	20.05	9.49	9.25	4.41	0.25	−0.78
GT8194048	1.38	20.45	11.62	10.42	4.31	0.43	−0.82
GT8194049	0.86	20.05	8.80	7.90	4.29	0.50	−0.60

Study Area: Tanore Upazilla

Figure 1. Schematic representation of the study area.

2.1.1. Missing Value Imputation

The collected data at the observation wells have a few missing entries that were imputed as a data pre-processing measure. There exist several approaches to fill the missing entries. The authors in [67] conducted a comparison of three methods for estimating missing entries for a dataset of gene microarray: Singular Value Decomposition (SVD)-based method—SVD imputes, weighted K-nearest neighbours—KNN impute, and row averaging method. They demonstrated the superiority of the KNN impute over the SVD impute and row average methods with respect to robustness and sensitivity for the estimation of missing entries. Therefore, this research adopted the KNN imputation method to fill the missing values of groundwater level data at the selected three observation wells. The algorithm for the K-nearest neighbour approach to impute missing entries presented in [68] was adopted in this research. The weekly values of the groundwater table time series data after imputation of the missing entries at the three observation wells are presented in Figure 2.
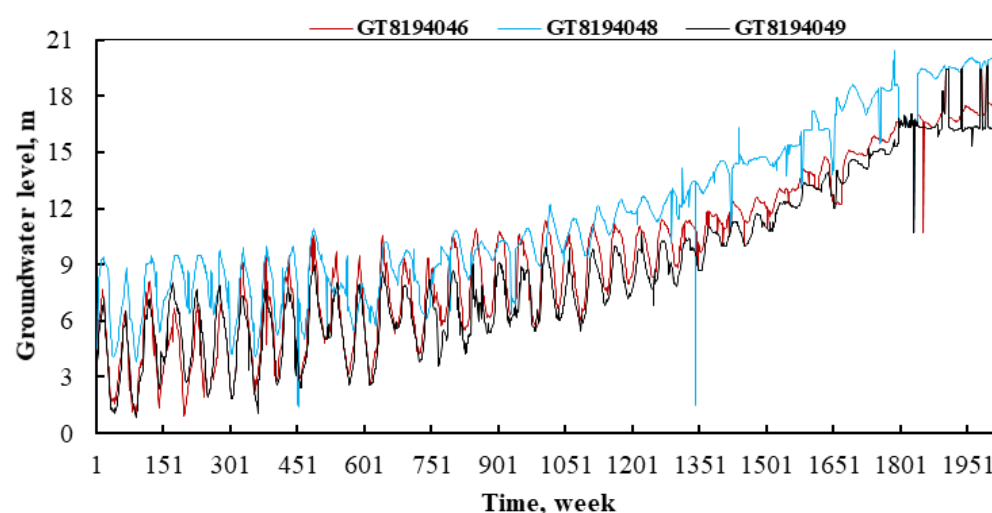
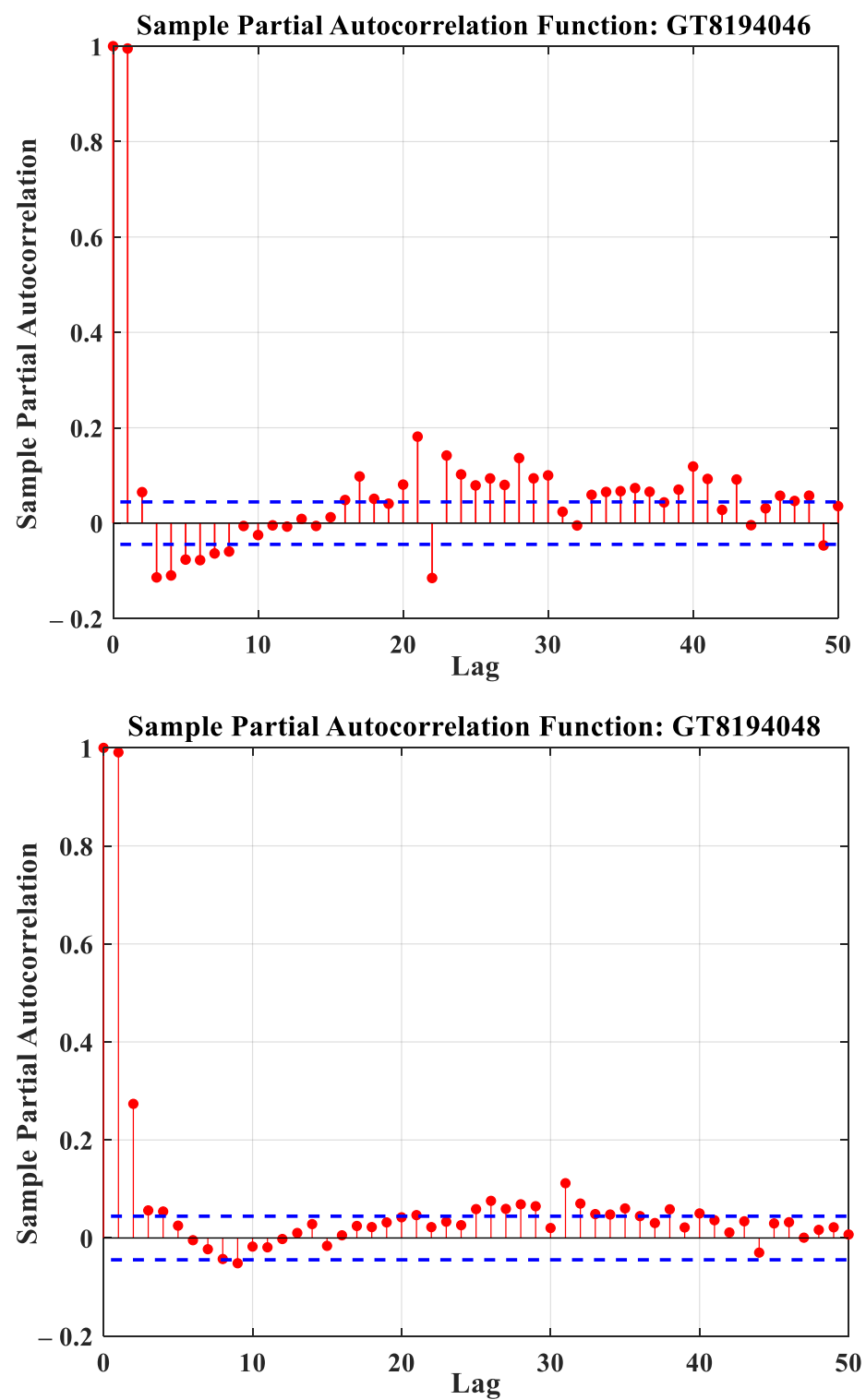**Figure 2.** Time series of the groundwater level data.

It is observed from Figure 2 that the groundwater level data at all three observation wells have some noisy data, especially at the later part of the time series. This noise in the input data was intentionally kept to evaluate the prediction power of the suggested machine-learning algorithms on the noisy input data. As such, no data smoothing operation was performed on the input time series (weekly values) of the groundwater level data.

2.1.2. Selection of Input Variables

The most significant and pertinent aspect in creating machine-learning-based prediction models should be the choice of suitable input variables from a list of candidate input variables that may enhance the prediction capability of models. As there exists no explicit approach to determining model inputs for data-driven modelling applications [69], several methods were adopted and applied by various researchers. It is also noted that useful input variable selection approaches are non-unique and different techniques may result in different combinations of important input variables [44]. A two-step approach can be adopted in selecting the most useful input variables [70]: utilization of Autocorrelation and Partial Autocorrelation Functions (PACF) (to obtain time-lagged information), followed by a "trial and error" approach, wherein several possible combinations of preselected lags can be used as model inputs. However, evaluating each of the combinations using several data-driven models to select the significant input variables is undoubtedly a time-consuming and laborious task. As an improvement to this laborious and computationally intensive input variable selection method, the present study adopts Frequentist Lasso Regression (FLR) [71] performed on the preselected lags (using PACF) for determining the most significant input variables. The proposed approach, utilizing the combination of PACF and the FLR, is outlined below:

1.   Partial autocorrelations (PACF)

The PACF approach was used to select significant inputs from the Groundwater Level (GL) lags. PACF functions at the selected observation wells were determined to acquire time-lagged statistics from the weekly time series data of GLs. This time-lagged information was used to evaluate the temporal dependencies between GL for a current week (GL_t) and the GLs at a certain point in an earlier period (i.e., a time lag of GL_{t-1}, GL_{t-2}, GL_{t-3}, GL_{t-4}, and GL_{t-5}, etc.). This temporal reliance in the GL time series at the observation wells was evaluated for 50 lags (i.e., from GL_{t-1} to GL_{t-50}) as depicted in Figure 3. In Figure 3, the 95% confidence band is indicated by the blue dashed lines. According to Figure 3, the relevant inputs to the prediction models for the GL time series at the three observation wells were initially determined.

Figure 3. *Cont.*

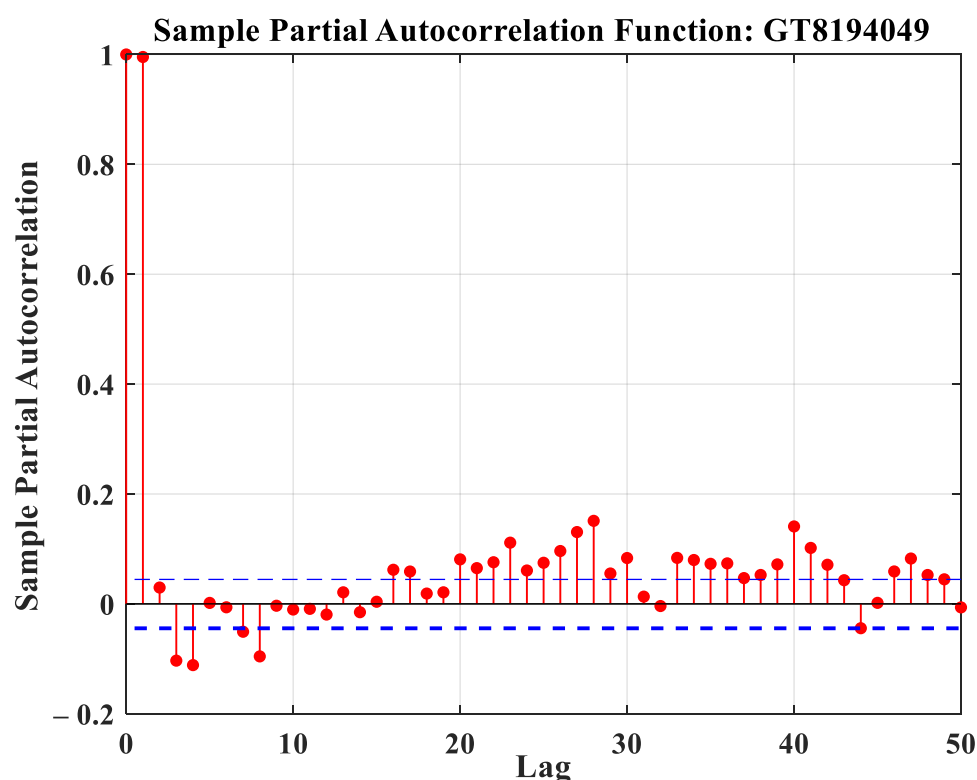**Sample Partial Autocorrelation Function: GT8194049**

Figure 3. Partial autocorrelation plots of the groundwater level time series for 50 lags (weeks) at the observation wells.

Thus, the input variables primarily determined based on the PACF criterion for the observation well GT8194046 include:

GL_t, GL_{t-1}, GL_{t-2}, GL_{t-3}, GL_{t-4}, GL_{t-5}, GL_{t-6}, GL_{t-7}, GL_{t-8}, GL_{t-16}, GL_{t-17}, GL_{t-18}, GL_{t-20}, GL_{t-21}, GL_{t-22}, GL_{t-23}, GL_{t-24}, GL_{t-25}, GL_{t-26}, GL_{t-27}, GL_{t-28}, GL_{t-29}, GL_{t-30}, GL_{t-33}, GL_{t-34}, GL_{t-35}, GL_{t-36}, GL_{t-37}, GL_{t-39}, GL_{t-40}, GL_{t-41}, and GL_{t-43}.

Input variables identified by PACF criterion at GT8194048 are:

GL_t, GL_{t-1}, GL_{t-2}, GL_{t-3}, GL_{t-4}, GL_{t-9}, GL_{t-21}, GL_{t-25}, GL_{t-26}, GL_{t-27}, GL_{t-28}, GL_{t-29}, GL_{t-31}, GL_{t-32}, GL_{t-35}, and GL_{t-38}.

Input variables identified by PACF criterion at GT8194049 are:

GL_t, GL_{t-1}, GL_{t-3}, GL_{t-4}, GL_{t-7}, GL_{t-8}, GL_{t-16}, GL_{t-17}, GL_{t-20}, GL_{t-21}, GL_{t-22}, GL_{t-23}, GL_{t-24}, GL_{t-25}, GL_{t-26}, GL_{t-27}, GL_{t-28}, GL_{t-29}, GL_{t-30}, GL_{t-33}, GL_{t-34}, GL_{t-35}, GL_{t-36}, GL_{t-39}, GL_{t-40}, GL_{t-41}, GL_{t-42}, GL_{t-46}, and GL_{t-47}.

Obviously, a substantial number of input variables were identified as potential input variables at the observation wells based on the PACF criterion. While using all of these input variables may provide better or worse (some of them being either redundant or misleading and may cause prediction inaccuracies) prediction accuracies, this inclusion of more input variables will no doubt incur an additional computational burden. On the other hand, evaluating various combinations of these input variables is computationally intensive, tedious, and time-consuming. Therefore, the present study strives to propose an approach named FLR to eliminate the redundant or less influential input variables from the pre-selected input variables. According to the conscious knowledge of the authors, this methodology of significant input variable selection has not been applied previously for groundwater level forecasting.

2.   Frequentist Lasso Regression (FLR)

The second phase of input variable selection was facilitated by FLR [71], categorized as a member of the Bayesian lasso regression. Lasso regression is basically an approach of performing a linear regression that integrates regularization and selection of variables.

The regularization part aids in preventing model overfitting by reducing the extent of the coefficients of regression. The FLR approach is different from other forms of regularization methods (i.e., ridge regression) with respect to the way of assigning values to regression coefficients. In the FLR technique, the regression coefficients corresponding to the redundant or insignificant variables are assigned a value of exactly 0 by the frequentist lasso. In this study, the FLR model was fit on the pre-selected (PACF selected) input variables and the one-week ahead groundwater level (GL_{t+1}) as the output variable for each of the observation wells. At GT8194046, 32 input variables based on different time lags were used as inputs, whereas 16 and 29 input variables were used at observation wells GT8194048 and GT8194049, respectively. The inputs and outputs at each observation well were divided into train and test datasets. On or about 80% of the entire data were used to train the FLR model, whereas the remaining 20% were used to test the model. The Forecast Mean Squared Error (FMSE) values were computed and the magnitude of regression coefficients (with respect to the shrinkage value) are plotted as illustrated in Figure 4. It is observed from Figure 4 that a model with 11 (df = 11), 5 (df = 5), and 9 (df = 9) input variables seemed to balance minimal FMSE and model complexity well at the observation wells GT8194046, GT8194048, and GT8194049, respectively. Then, the coefficients that correspond to the models containing 11, 5, and 9 input variables were computed that provided minimal FMSE at each case. The FLR suggests that the input variable combinations outlined in Table 2 were the most useful in determining the one-week ahead groundwater level predictions. The variables other than those mentioned in Table 2 were either redundant or insignificant. The input variables other than the above-mentioned ones had an exact value of 0 for the regression coefficient. This study used statistical approaches for input variable selection, which can also be performed by employing an evolutionary algorithm along with the parameter tuning process of the prediction models.

To eliminate the adverse effect of the data's dimensionality, standardization was performed to scale the data to a mean of zero and a standard deviation of unity [72]. The standardized data hold the actual data shape features, including the skewness and kurtosis values.
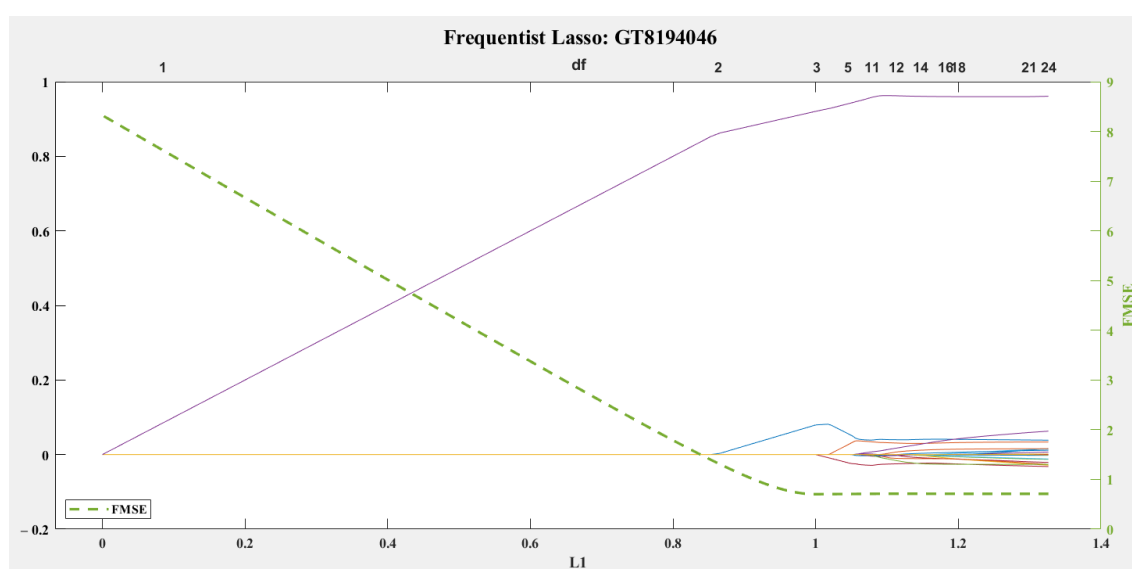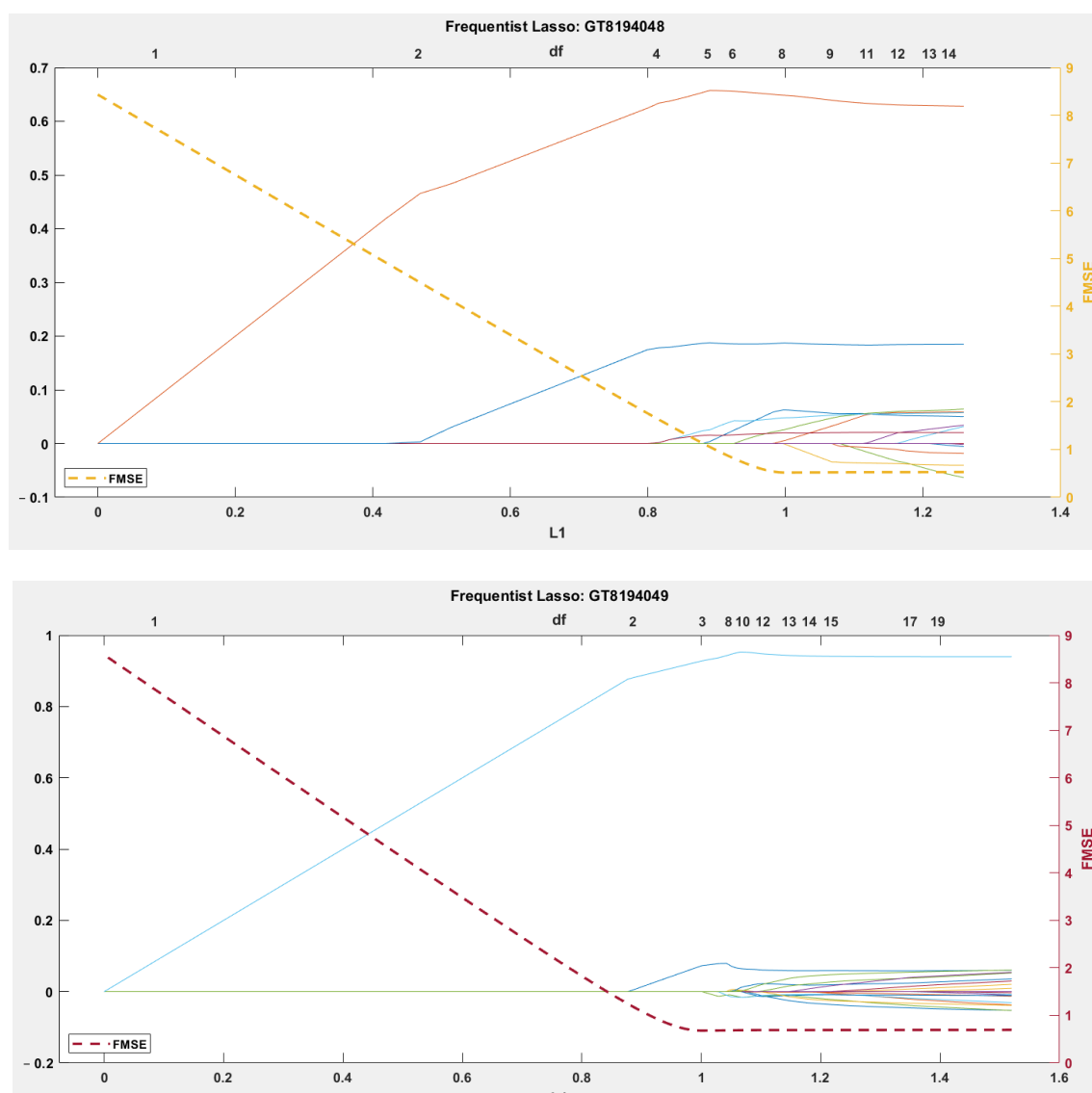

Figure 4. *Cont.*

Figure 4. The magnitude of the Frequentist Lasso Regression coefficients with respect to the shrinkage values at the observation wells (FMSE = forecast mean squared error).

Table 2. Input variables determined by the df of frequentist lasso regression.

Observation Wells	Input Variables Combination
GT8194046	GL_t, GL_{t-2}, GL_{t-6}, GL_{t-7}, GL_{t-17}, GL_{t-18}, GL_{t-24}, GL_{t-29}, GL_{t-39}, GL_{t-41}, GL_{t-43}
GT8194048	GL_t, GL_{t-1}, GL_{t-2}, GL_{t-3}, GL_{t-38}
GT8194049	GL_t, GL_{t-1}, GL_{t-8}, GL_{t-17}, GL_{t-20}, GL_{t-33}, GL_{t-36}, GL_{t-40}, GL_{t-42}

2.2. Prediction Model: Adaptive Neuro Fuzzy Inference System (ANFIS)

An ANFIS is a flexible and adaptive data-driven machine-learning tool that holds the advantageous features of both a Fuzzy Inference System (FIS) developed from fuzzy logic theory and an ANN system. It incorporates fuzziness, imprecision, or nebulousness of input datasets in modelling complex and nonlinear mapping of input–output patterns of a dataset [73]. For this capability, ANFIS-based prediction models are often referred to as the universal approximators of a complex system [74,75]. Among various types of ANFIS models, a Sugeno type can provide a comparatively better prediction through superior learning ability despite having a rather simple model architecture [73]. For this reason, this

research adopted a Sugeno-type ANFIS model. Sugeno-type ANFIS models are developed from an initial FIS structure, the parameters of which needed to be tuned using a preferable optimization algorithm. The number of tuneable or modifiable parameters (both linear and nonlinear) depends on the number of input variables for a specific problem. The higher the number of modifiable parameters, the more complex the ANFIS model will be, and consequently, the higher the computational requirements. Therefore, an additional step of reducing the dimensionality of the input space is generally adopted to develop an ANFIS model. The present study employed a Fuzzy C-Mean Clustering (FCM) [76] algorithm to reduce the training dataset's dimensionality. This FCM approach significantly reduces the computational requirements by minimizing the number of linear and nonlinear modifiable parameters of an ANFIS model architecture. The modelling was performed by utilizing input and output Membership Functions (MFs), which were Gaussian and linear, respectively. The input Gaussian MF is expressed by two parameters (c, σ) and can be denoted by [73]:

$$gaussian\ (x, c, \sigma) = e^{-\frac{1}{2}\left(\frac{x-c}{\sigma}\right)^2} \tag{1}$$

where c and σ represent the centre and width, respectively of the MFs. The building block of an ANFIS architecture derived from a Sugeno-type FIS is graphically shown in Figure 5.
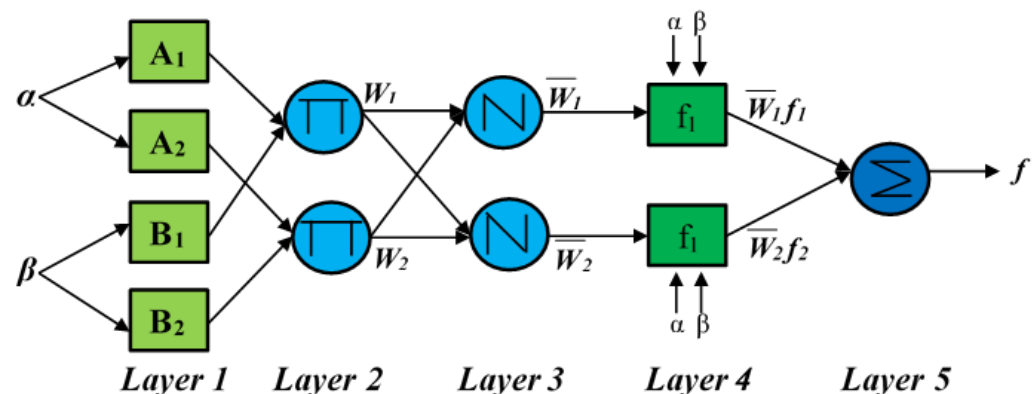

Figure 5. ANFIS structure derived from two inputs—one output first-order Sugeno FIS [77].

The Sugeno FIS illustrated in Figure 5 has two inputs (α and β) and one output (f), the fuzzy if-then rule sets for them can be written as:

$$Rule\ 1 : If\ \alpha\ is\ A_1\ and\ \beta\ is\ B_1\ then\ f_1 = p_1\alpha + q_1\beta + r_1 \tag{2}$$

$$Rule\ 2 : If\ \alpha\ is\ A_2\ and\ \beta\ is\ B_2\ then\ f_2 = p_2\alpha + q_2\beta + r_2 \tag{3}$$

As can be seen from Figure 5, a Sugeno-type ANFIS is composed of five layers: (1) fuzzy layer, (2) product layer, (3) normalized layer, (4) defuzzification layer, and (5) output layer. Each layer is associated with a particular task as the model development progresses. These layers are described in detail along with their functions in [77] and are not repeated in this study. MATLAB commands and functions were used to develop the ANFIS-based prediction models.

2.3. Algorithms to Tune ANFIS Parameters

2.3.1. Hybrid Algorithm (HA)

One of the major issues that arise when developing fuzzy logic-based models with high-dimensional data is selecting the appropriate rule sets, which largely determine the optimal model performance. This issue can be addressed adequately by adopting a first-order Sugeno FIS (presented in Figure 5), which is capable of learning adaptively through modifying the rule sets, thus providing an optimal parameter set for the FIS model. The basic learning rules of a flexible and modifiable (adaptive) network are made up of two components: gradient descent and chain rule [78]. A gradient method is

usually exploited to tune parameters of the antecedent and consequent components of the rule base. This gradient approach results in slow convergence of the tuning process and is prone to become trapped in local optima instead of global optima. To overcome these issues of slow convergence and infeasible solutions, a "hybrid learning rule" that integrates Gradient Descent (GD) and Least Squares Estimates (LSE) is proposed to search for optimal FIS parameters [77]. In a FIS rule base, the antecedent parameters are regarded as nonlinear in nature, whereas the consequent parameters are linear. In the hybrid algorithm proposed by [77], the antecedent parameters are computed by means of the GD via error backpropagation, while the recursive LSE determines the consequent parameters. This integration of GD and LSE in parameter tuning of ANFIS models is referred to as a Hybrid Algorithm (HA), which employs a frontward and a rearward pass to perform the hybrid learning method. In this study, the HA was employed to tune the parameters of a traditional ANFIS model.

Various hybridized ANFIS models have been widely applied to various research domains for improving the performance of the traditional ANFIS models. However, the use of evolutionary algorithm tuned ANFIS models has not been observed in recent literature to predict groundwater level fluctuations (daily or multiple steps ahead prediction). As a pioneering effort, this research proposes the hybridized learning of ANFIS models using Differential Evolution (DE) and Particle Swarm Optimization (PSO) to forecast one- and multi-week-ahead groundwater levels at the selected observation wells. A brief description of DE and PSO is provided in the following sub-sections.

2.3.2. Differential Evolution (DE)

The DE algorithm [79,80] is a stochastic and population-inspired optimization algorithm that is ideally suited for providing solutions to numerous nonlinear optimization formulations. The concept of DE is simple, with a fundamental configuration of DE/rand/1/bin [81,82]. In DE, a preliminary set of the population is arbitrarily created following a uniform distribution with the specified lower and higher bounds of x_j^L and x_j^U, respectively. This randomly created initial population contains NP vectors such that X_i, $\forall_i = 1, 2, 3, \ldots, NP$. Following this initialization, the created individuals are evolved by mutation and crossover operators, resulting in the production of a trial vector. The resulting trial vector is compared to the associated parent to determine which vector should be passed on to the subsequent cohort of the population [83]. The basic steps of the DE algorithm consist of initialization, mutation, crossover, and selection. The details of these steps can be found in [83] and are not repeated here.

2.3.3. Particle Swarm Optimization (PSO)

The PSO [84], a population-inspired stochastic algorithm for solving optimization problems, is stimulated by social and psychological principles. The PSO is derived from swarm intelligence principles, which simulate the societal characteristics of bird flocking or fish schooling predation. The algorithm has acquired popularity as a result of its numerous advantageous properties, including its simple structure, robust manoeuvrability, and ease of implementation [85], which makes it ideal for training various intelligent models. PSO considers each particle as a possible solution inside the search domain of an optimization problem. On the other hand, the flight behaviour of the particles is recognized as an individual's exploration phenomenon. In PSO, the dynamic update of a particle's velocity is determined by the particle's previous optimal location and the swarm population.

PSO considers the values of the particle's objective function to be the corresponding fitness values. These fitness values are used to calculate the particles' optimal position. The fitness values are also utilized to update the particles' past most advantageous location and the swarm population's optimum location. Thus, the PSO algorithm's control parameters determine the convergence of particles trajectories [85]. The PSO algorithm converges by keeping records of each particle's best fitness values, finding the global best particle, and updating the locations and velocities of each particle. In the event that the convergence is

not achieved, the iterative process continues until the optimization problem converges to its optimal solution, or until the user-defined maximum number of iterations is satisfied.

2.4. Developed ANFIS Models

The parameters of the ANFIS model were tuned using the HA and two population-based optimization algorithms, e.g., DE and PSO, to develop the optimized ANFIS models (HA-ANFIS, DE-ANFIS, and PSO-ANFIS, respectively). Performances of the tuned ANFIS models principally be subjected to the optimal tuning for the parameters of the algorithms. These parameters were selected upon conducting several trials and the best parameters were used for the developed models. The optimum parameter sets used to train the hybridized ANFIS models are depicted in Table 3.

Table 3. Optimal parameter values for the selected optimization algorithms.

Algorithms	Optimal Parameter Values	
DE	Maximum number of iterations: 1000 Number of populations (colony size): 100 Lower bound of scaling factor: 0.2 Upper bound of scaling factor: 0.8 Crossover probability: 0.2	
PSO	Maximum number of iterations: 200 Population size (Swarm size): 100 Inertia weight: 1 Inertia weight damping ratio: 0.99 Personal learning coefficient: 1 Global learning coefficient: 2 Maximum velocity: 1 Minimum velocity: −1	
HA	*FIS parameters* Fuzzy partition matrix exponent: 2.0 Maximum number of iterations: 1000 Minimum improvement: 1×10^{-5}	*ANFIS parameters* Maximum number of Epochs: 200 Error goal: 0 Initial step size: 0.01 Step size decrease rate: 0.9 Step size increase rate: 1.1

HA-ANFIS, DE-ANFIS and PSO-ANFIS models were developed at each observation well to predict one-week-ahead groundwater levels. The input variables to the models were the selected lagged groundwater level values and the outputs from the models were the one-week ahead groundwater levels. Both parameters (antecedent and consequent) of the initial FIS models were tuned using the HA, DE and PSO algorithms to find the ideal HA-ANFIS, DE-ANFIS and PSO-ANFIS models. Different combinations of antecedent and consequent parameters were evaluated by the HA, DE and PSO algorithm as the training process progressed. The Mean Squared Error (MSE) reflecting the learning error was employed as the cost function of the HA, DE, and PSO-based optimization approach. The overall goal or aim was to minimize the MSE values between the observed (actual) and model-predicted groundwater levels on the training set of the data. The cost function (objective function) can be represented mathematically as:

$$Minimize : f(GL_{MSE}) = \frac{\sum_{i=1}^{n} \left(GL_{i,a} - GL_{i,p} \right)^2}{n} \tag{4}$$

where, $f(GL_{MSE})$ denotes the cost function (objective function) to be minimized; $i = 1, 2, 3, \dots, n$ denotes the quantity of training dataset; $GL_{i,a}$ is the actual groundwater levels in the training set of the data; and $GL_{i,p}$ is the model-predicted groundwater level values in the training set of data.

The properly trained optimized models were then presented with the test dataset and the testing errors were computed. The performances of the DE-ANFIS and PSO-ANFIS were weighed against those of the traditional ANFIS model (HA-ANFIS).

2.5. Training of Optimized ANFIS Models

The performance of a classical ANFIS model (HA-ANFIS) whose parameters were tuned with a HA (integration of LSE and GD) was used as a base model for settling on the adequate number of clusters determined via the FCM algorithm. A clustering trial was performed using a range of clusters between 2–10 for the HA-ANFIS models with 50% training data and 50% test data. Absolute differences between the training and test RMSE, including the absolute difference between train and test R values, were used as the selection criteria for the number of clusters. Based on the trial, two clusters produced the best results for the HA-ANFIS models at observation wells GT8194046 and GT8194048, respectively, whereas the number of clusters that have the best results at GT8194049 was three. The same quantity of clusters (FCM) was used for the evolutionary algorithm-tuned ANFIS models (DE-ANFIS and PSO-ANFIS). The resulting architectures for five inputs (as in the case of GT8194048) and one output HA-ANFIS models are presented in Figure 6.
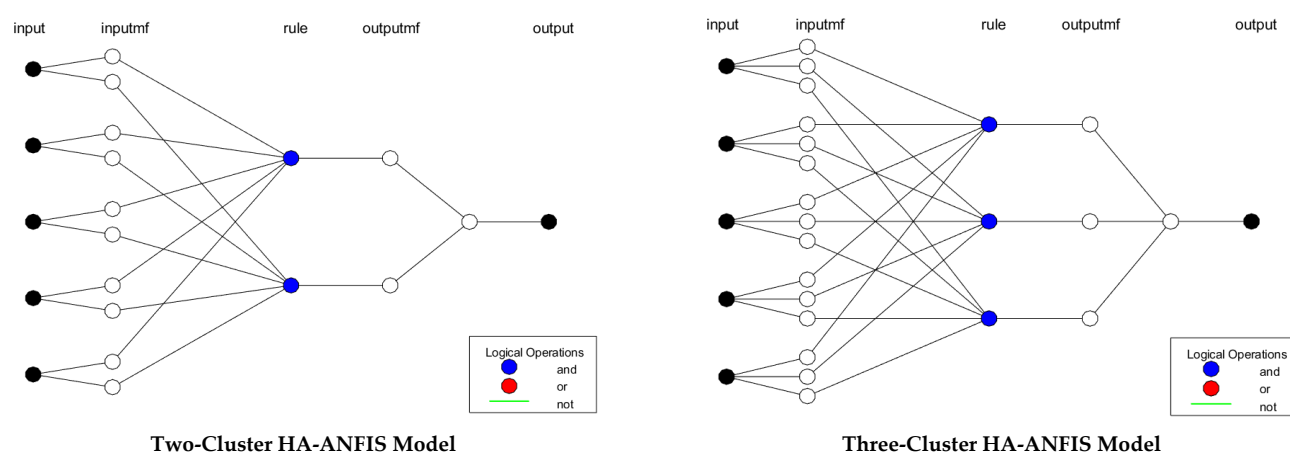

Two-Cluster HA-ANFIS Model　　　　　　　　**Three-Cluster HA-ANFIS Model**

Figure 6. Model architectures of the developed HA-ANFIS models.

Training and test errors (RMSE values) were calculated for each of the developed optimized ANFIS models, and the training time was recorded. Training and test errors are important criteria to ensure that the developed models are not over- or under-trained. Model training time is another imperative criterion that needs to be observed and considered carefully. Models requiring longer training time may sometimes be infeasible when dealing with complex problems with larger datasets. The training and test errors as well as the time of training needed for the optimized ANFIS models at different observation wells are presented in Table 4.

Table 4. Training RMSE, test RMSE, and training time required for training of the hybridized ANFIS models.

ANFIS Models	GT8194046			GT8194048			GT8194049		
	Train RMSE, m	Test RMSE, m	Training Time, min	Train RMSE, m	Test RMSE, m	Training Time, min	Train RMSE, m	Test RMSE, m	Training Time, min
DE-ANFIS	0.3565	0.4877	413	0.4485	0.7610	144	0.3453	0.5026	622
PSO-ANFIS	0.3382	0.5332	83	0.4389	0.8965	27	0.3109	0.4846	117
HA-ANFIS	0.3382	0.5089	0.60	0.4270	0.6761	0.36	0.3123	0.4578	0.45

The results presented in Table 4 indicate that the DE-ANFIS performed better than the PSO-ANFIS and the HA-ANFIS, with respect to test RMSE and the absolute difference between the training and test RMSEs at GT8194046. On the other hand, the HA-ANFIS was the best performing model followed by the DE-ANFIS and the PSO-ANFIS at the observation wells GT8194048 and GT8194049 when the absolute difference between the training and test RMSEs was considered. However, based on the test RMSE, the sequence of models from the best to the worst at GT8194048 was the HA-ANFIS, the DE-ANFIS, and the PSO-ANFIS, while this sequence at GT8194049 was the HA-ANFIS, the PSO-ANFIS, and the DE-ANFIS. It is also obvious from Table 4 that the training times required to train the HA-ANFIS models were almost negligible compared to those of the DE-ANFIS and PSO-ANFIS models, and that the PSO-ANFIS required less training time than DE-ANFIS. Therefore, it can be argued that the HA-ANFIS was the best model with respect to the RMSE and training time criteria. Other performance evaluation indexes were calculated on test results for the comparison purpose of the developed optimized ANFIS models. The performance evaluation indexes employed to evaluate the prediction performances of all standalone optimized ANFIS models, and their ensemble are given in Appendix A.

2.6. Weight Calculation

For developing a framework of ensemble prediction, weights of the individual prediction models were calculated. Both the benefit and cost indexes were employed to compute weights for the developed models, mainly to incorporate the conflicting nature of performances by the prediction models for different performance indexes calculated on the test dataset. The benefit indexes considered for the weight calculation were Coefficient of Determination (R^2), Willmott's Index of Agreement (IOA), and Nash–Sutcliffe Efficiency Coefficient (NS), whereas the cost indexes selected were Root Mean Squared Error (RMSE), Maximum Absolute Error (MAE), and Median Absolute Deviation (MAD). An optimization approach, MOGA was applied to determine the associated weights of individual prediction models based on their performances, with respect to the selected performance indexes. For the benefit and cost indexes, the weight coefficients X_1–X_3 were assigned for the prediction models DE-ANFIS, PSO-ANFIS, and HA-ANFIS, respectively. Two conflicting objectives were considered: (1) maximize the sum of benefit indexes for each of the prediction models, and (2) minimalize the summation of the cost indexes for each of the prediction models. The mathematical formulation of the proposed MOGA-based weight assignment scheme can be represented as:

$$Maximize : \ f_1(BI) = \sum_{i=1}^{N} X_i^n \times \sum_{j=1}^{K} BI^k \tag{5}$$

$$Minimize : \ f_2(CI) = \sum_{i=1}^{N} X_i^n \times \sum_{l=1}^{L} CI^l \tag{6}$$

Subject to

$$BI(min) \leq BI^k \leq BI(max) \tag{7}$$

$$CI(min) \leq CI^l \leq CI(max) \tag{8}$$

$$X_i^n \geq 0 \tag{9}$$

$$\sum_{i=1}^{N} X_i^n = 1 \tag{10}$$

where, $f_1(BI)$ is the objective function that represents the maximization of the sum of benefit indexes; $f_2(CI)$ represents the objective function that describes the minimization of the sum of cost indexes; X_i^n. is the ith eight coefficient of the nth model; BI^k is the kth benefit index ($K = 3$); CI^l is the lth cost index ($L = 3$); Equations (7) and (8) represent the lower and upper limits of the benefit and cost indexes, respectively; Equation (9) designates

the non-negativity of the ith weight coefficient; Equation (10) indicates the sum of the ith weight coefficient equals 1; N, K, and L stand for a total number of prediction models, benefit indexes, and cost indexes, respectively. Equation (5) represents the maximization of the sum of benefit indexes, whereas Equation (6) represents the minimization of the sum of cost indexes.

The MOGAs provide a set of feasible solutions represented by a Pareto optimal front instead of providing a single solution. Each of the solutions in the Pareto front is regarded as a feasible solution. The single best possible solution from the Pareto front was selected by applying the concept of Grey Relational Analysis (GRA), which is derived from the Grey System Theory [86]. In this approach, Gray Relational Coefficient (GRC) [84] is computed to obtain the best feasible optimum solution from a set of feasible solutions in the Pareto front. The GRC approach finds the similarity between the objective values of the individual optimal solutions and the ideal or best reference objective value. The computation of GRC was performed following the steps used in [87]. Based on the GRA concept, the greater the value of GRC_i is, the more dependable the optimal solution will be. Therefore, the largest value of GRC_i was the recommended best optimal solution from the Pareto optimal solution. The corresponding weight coefficients for the best optimal solution were assigned to the standalone optimized ANFIS models to develop the ensemble.

2.7. Ensemble Prediction

An ensemble approach of prediction modelling is generally preferred because an individual prediction model often fails to capture the associated input-output relationships and map the true trends of these associations within the reasonable locations of the input domain [88]. An ensemble prediction model improves prediction robustness by extracting the true trends of the input-output relationships in the data and protecting against an individual poor-performing model by minimizing the impact of poor predictions by that prediction model [46]. Ensemble prediction models provide better accuracy than the individual models because the ensembles utilize the distinctive characteristics of individual models for capturing various patterns of the input-output relations or mappings from the whole decision domain. Nevertheless, individual models for an ensemble need to be sufficiently diverse and sensibly precise in their prediction abilities. The optimal number of individual models in an ensemble is highly dependent on the trade-offs between model complexity, prediction accuracy, and uncertainty reduction level. An ensemble prediction is simply computed by:

$$Output_{EN} = \sum_{i=1}^{n} \frac{Output_i^{IM}}{n} \tag{11}$$

where, $Output_{EN}$ is the ensemble output; $Output_i^{IM}$ represents the outputs of the ith single model; n is the number of single models to be used for the ensemble formation.

This simple ensemble modelling approach generally assigns equal weights to all individual models regardless of their prediction accuracies. A more precise ensemble formation technique is the weighted average approach, which is likely to yield the best correlation between the observed and model-predicted responses [46]. In this concept, more accurate prediction models are given higher weightage and the less accurate models receive lower weights. In contrast, the sum of weights assigned to all individual models must be equal to 1. The weighted average ensemble approach may be mathematically denoted by the following deterministic function:

$$Y_{WA}(x) = \sum_{i=1}^{n} \omega_i(x) \times Y_{IM_i}(x) \tag{12}$$

where, x represents the input space; Y_{WA} is the prediction of the weighted average ensemble with respect to x; ω_i is the numeric value of weight allotted to ith individual model; Y_{IM_i} is the prediction of the ith single model; n is the number of single models to be used for the ensemble formation. The ensemble thus obtained is adaptive in nature because the weights are a function of x [50]. This adaptive weighted average ensemble approach was adopted in this research wherein the assigned weights were calculated using a MOGA.

Once the ensemble prediction was obtained, the corresponding performance indexes were calculated for the ensemble model for comparison purposes with the individual models. Then, a decision theory was applied by incorporating the same benefit and cost indexes as in the case of the MOGA-based weight assignment scheme. In this case, the ensemble model's performance indexes were also considered to provide a ranking of all individual models and the ensemble. The decision theory employed in this study was the Shannon's entropy [51]. The phases or steps adopted in [89,90] were used to calculate the entropy-based weights. The calculation steps are provided in Appendix A.

3. Results and Discussion

The study aims at providing a comparison of the three machine-learning algorithms, DE-ANFIS, PSO-ANFIS, and HA-ANFIS for predicting one- and multi-week ahead groundwater levels using the previous lags as the input variables. A weighted-average ensemble of these prediction models is also developed, and precision in the prediction of the ensemble model is weighed against the prediction accuracy of the individual prediction models.

3.1. Prediction of Individual Models

After satisfactory training of the proposed prediction models, results are evaluated with respect to various performance evaluation indexes computed on the actual and predicted test datasets. The model predictions at different observation wells are presented in Figures 7–9 in the form of hydrographs and scatterplots.

It is observed from the hydrographs and scatterplots presented in Figure 7 that at GT8194046, the DE-ANFIS predictions have better agreement with the actual groundwater level values when compared to other models. The other models face difficulties capturing the true trends in the groundwater level fluctuations, especially at the later parts of the time series (higher values of groundwater level fluctuations), which are underestimated by the PSO-ANFIS and HA-ANFIS models. The PSO-ANFIS appears to be the worst performing model at this observation well.

The hydrograph of the HA-ANFIS (Figure 8) indicates the best matching between the actual and predicted groundwater levels at GT8194048. The prediction results of DE-ANFIS, for this instance, are the second-best, followed by the prediction outcomes of the PSO-ANFIS. PSO-ANFIS overestimates the actual groundwater level fluctuations that begin at the middle of the time series and continue until the end. In contrast, the DE-ANFIS slightly overestimates the actual values.

At GT8194049 (Figure 9), the hydrographs indicate the similar prediction accuracies of the DE-ANFIS, PSO-ANFIS, and HA-ANFIS with the slightly better accomplishment of the HA-ANFIS model. The performance results for the one-week-ahead groundwater level predictions on the test dataset are provided in Table 5.
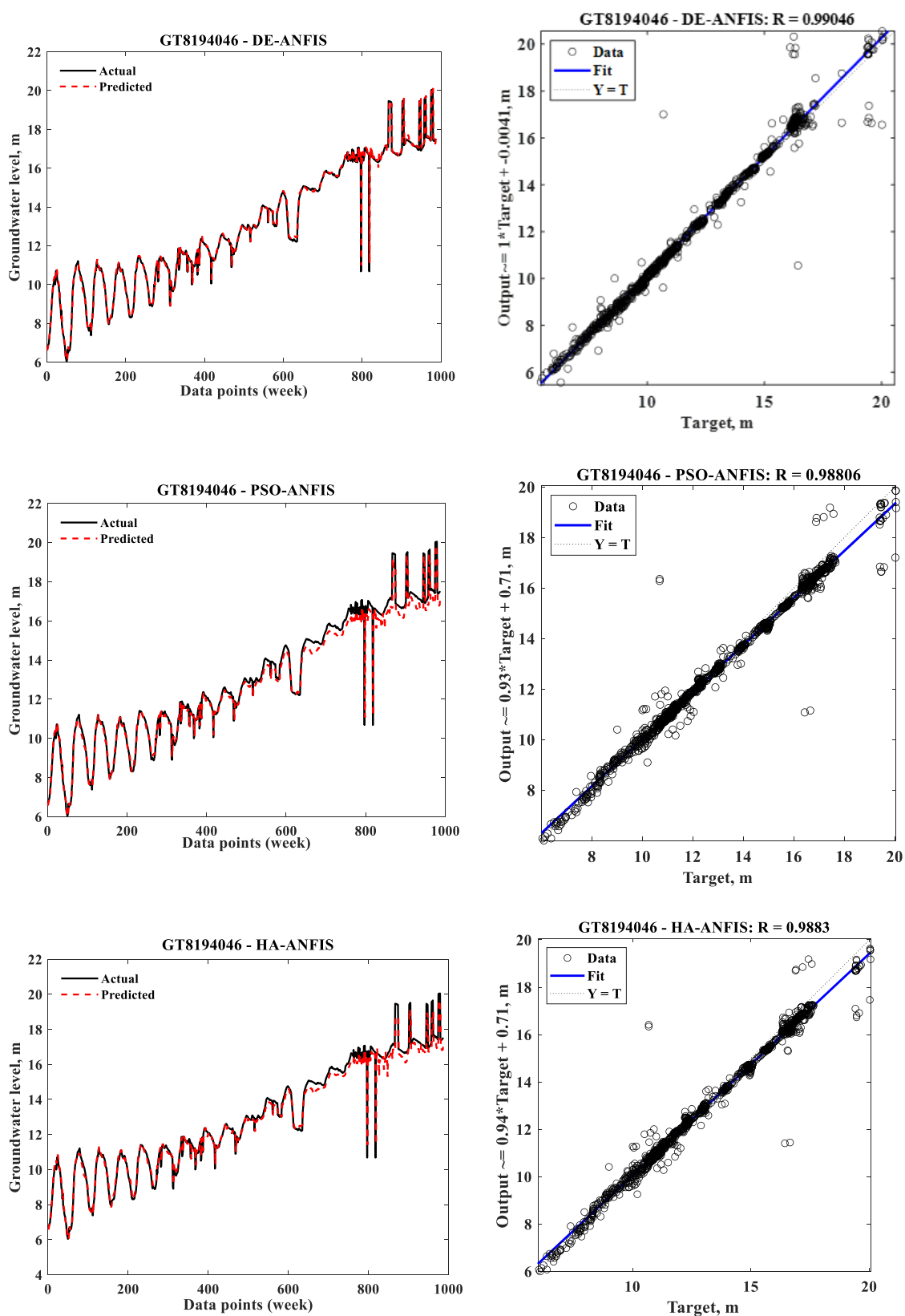
Figure 7. Actual and model predicted weekly groundwater level fluctuations and regression plots on the test dataset at the observation well GT8194046.
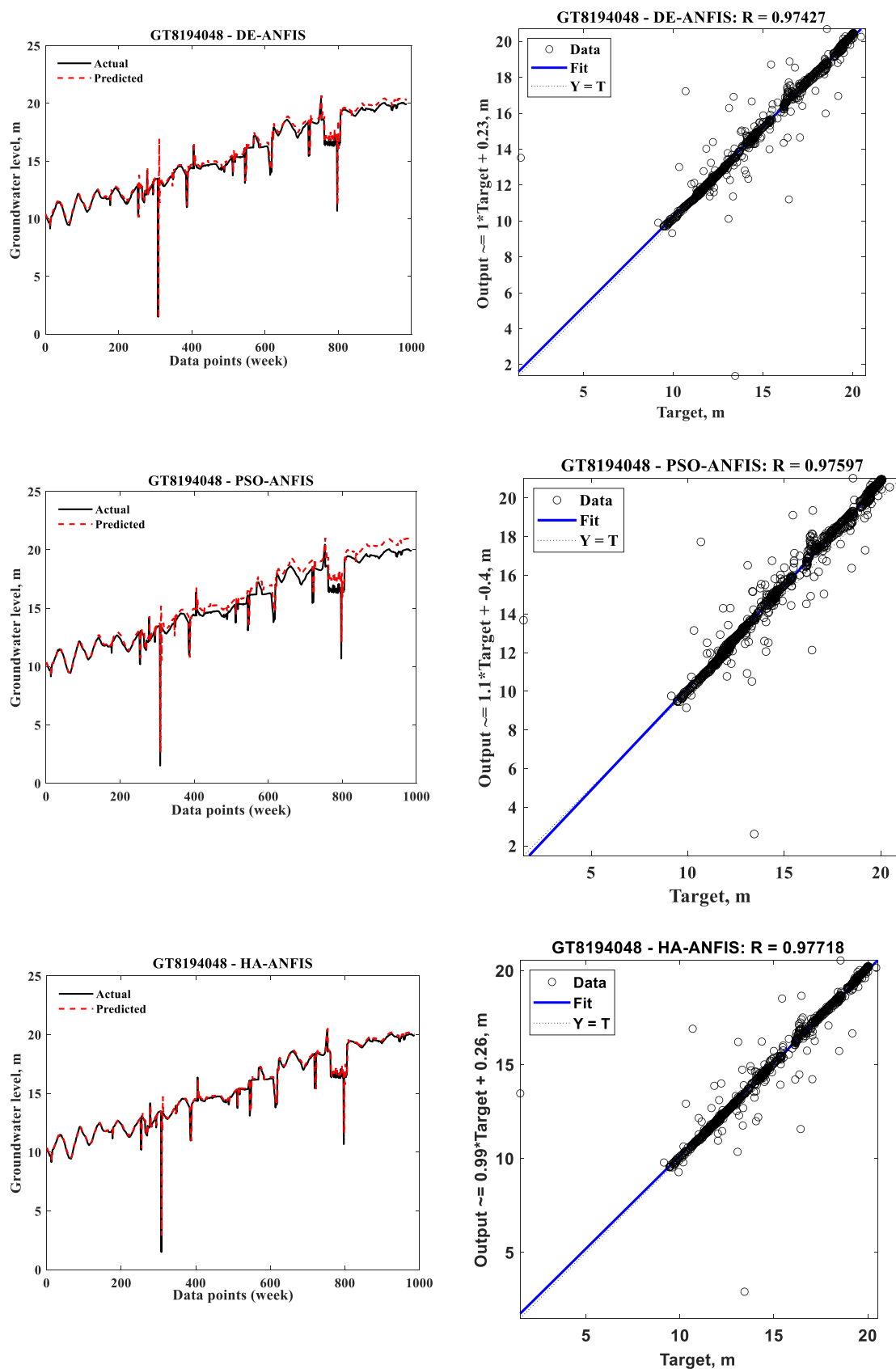
Figure 8. Actual and model predicted weekly groundwater level fluctuations and regression plots on the test dataset at the observation well GT8194048.
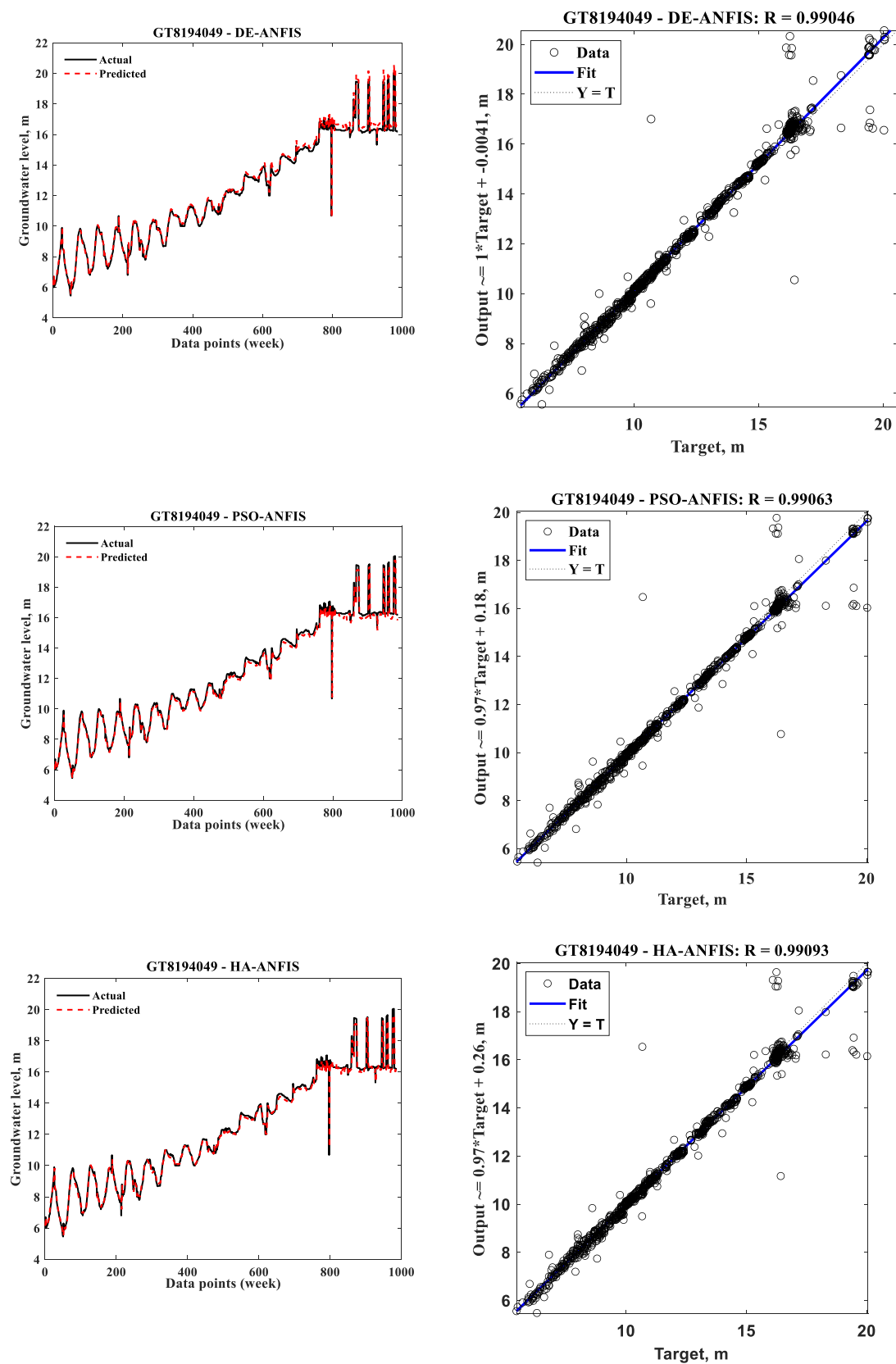
Figure 9. Actual and model predicted weekly groundwater level fluctuations and regression plots on the test dataset at the observation well GT8194049.

Table 5. Performance evaluation indexes of the proposed prediction models on test data at the observation wells.

PEI	GT8194046			GT8194048			GT8194049		
	M1	**M2**	**M3**	**M1**	**M2**	**M3**	**M1**	**M2**	**M3**
RMSE	0.488	0.533	0.509	0.761	0.897	0.676	0.503	0.485	0.458
rRMSE	0.038	0.041	0.039	0.050	0.059	0.045	0.041	0.039	0.038
R^2	0.976	0.976	0.977	0.950	0.953	0.955	0.981	0.981	0.982
MAE	6.148	5.675	5.736	12072	12.178	11.966	6.323	5.794	5.861
MAD	0.045	0.130	0.112	0.105	0.275	0.155	0.081	0.066	0.062
IOA	0.994	0.992	0.993	0.985	0.981	0.988	0.995	0.995	0.995
NS	0.976	0.971	0.973	0.940	0.917	0.953	0.978	0.979	0.981
a-10 index	0.980	0.985	0.984	0.978	0.973	0.979	0.981	0.981	0.981

PEI = Performance evaluation index, M1 = DE-ANFIS, M2 = PSO-ANFIS, M3 = HA-ANFIS.

The prediction outcomes presented in Table 5 indicate that all of the proposed prediction models are effective at predicting groundwater levels at week $t + 1$ (GL_{t+1}) as indicated by the various performance evaluation indexes. While no individual model performs the best at all observation wells, individual models approximate groundwater levels better than others. In general, all prediction models at the observation wells have satisfactory accuracy as all models have higher values R^2, IOA, NS, and a-10 index and lower RMSE, rRMSE, MAE, and MAD values. All models provide the worst prediction for the dataset at the observation well GT8194048, while the models developed using the datasets at the observation wells GT8194046 and GT8194049 provide better prediction accuracies with the best results obtained for the models developed at GT8194046. This may be because groundwater level datasets at GT8194046 have the lowest skewness value (0.25) compared to the skewness values at GT8194048 and GT8194049.

The prediction outcomes of the proposed prediction models are also assessed with reference to the Theil inequality statistics (U) and the global performance index (GPI). The evaluation results are presented in Table 6.

Table 6. Components of the Theil inequality statistics and global performance index values for prediction models on test data at the observation wells.

PEI	GT8194046			GT8194048			GT8194049		
	M1	**M2**	**M3**	**M1**	**M2**	**M3**	**M1**	**M2**	**M3**
U	0.018	0.020	0.019	0.024	0.028	0.022	0.020	0.019	0.018
U^B	0.004	0.119	0.063	0.099	0.284	0.015	0.105	0.102	0.025
U^V	0.001	0.112	0.106	0.012	0.085	0.003	0.025	0.015	0.018
U^C	0.995	0.769	0.831	0.888	0.631	0.982	0.870	0.883	0.957
MBE	0.031	−0.184	−0.128	0.241	0.478	0.083	0.163	−0.155	−0.072
T_{stat}	1.971	11.521	8.143	10.473	19.772	3.862	10.754	10.585	5.029
U_{95}	6.197	6.031	6.034	6.380	6.632	6.292	6.731	6.591	6.582
GPI	0.004	−0.162	−0.074	0.622	2.667	0.061	0.112	−0.098	−0.019

PEI = Performance evaluation index, M1 = DE-ANFIS, M2 = PSO-ANFIS, M3 = HA-ANFIS.

The U statistics and its components contain useful information on the relative accuracy of each prediction model and the plausible sources of prediction imprecision. The first element U^B is a measure of errors relating to the bias, the second element U^V quantifies the skill of the prediction models to replicate the degree of inconsistency or variability, and the third (last) element U^C enumerates the amount of chaotic error generated by various predictions. It is observed from Table 6 that U^C component constitutes a major part of errors produced by all the prediction models and at all the observation wells. Relatively lower values of U^B, U^V and U produced by the prediction models at the observation wells reveal that methodical error and bias is not a problem for the obtained predictions for the developed models.

To further appraise the performances of the developed models, the GPI criterion is employed, which evaluates the model performance skill by combining the impacts of MBE, RMSE, U_{95}, t-stat, and R^2 values in the prediction accuracy. The MBE index indicates whether the developed prediction model over- or under-estimates the groundwater level predictions at the observation wells. Positive values of MBE mean that the prediction model under-estimates the observed groundwater level data, while the negative value indicates an over-estimation of the observed groundwater level data. The t-stat [91] criterion and the RMSE and MBE criteria measure the closeness of the actual and predicted groundwater level values, thus offering a relatively more complicated evaluation of model performance. The U_{95} criterion measures a models' predictive deviations within the 95% confidence band [92,93]. The U_{95} values produced by the prediction models are within acceptable limits, varying only slightly at all the observation wells. The t-stat values differ substantially among the prediction models and at the observation wells: at GT8194046, DE-ANFIS has the lowest value of t-stat; at GT8194048, the HA-ANFIS has the lowest value of t-stat; and at GT8194049, the HA-ANFIS has the lowest value of t-stat. The MBE, RMSE, U95, t-stat, and R^2 values are used to compute the values of the GPI index. The reliability of a model is reversely proportionate to the absolute values of GPI (negative values of GPI originate from the negative MBE values), i.e., the lower the numeric value of the GPI index, the higher the accuracy of the prediction model and the other way around. Based on the GPI index, the DE-ANFIS is the best performer among others at GT8194046, while the HA-ANFIS is the best prediction model at both the observation wells GT8194048 and GT8194049.

It is perceived from Tables 5 and 6 that models show varying accuracies depending on the performance evaluation matrix computed on the actual and predicted groundwater level values. This means a contradiction in the prediction performance when different performance evaluation indexes are used. For instance, at GT8194046, one can select DE-ANFIS as the best model when RMSE, MAD, IOA, and NS are considered (Table 5). However, the HA-ANFIS and the PSO-ANFIS perform better with respect to R^2 and MAE criteria, respectively. At GT8194048, the HA-ANFIS has the better performance based on the RMSE, R^2, MAE, IOA, and NS criteria, whereas the DE-ANFIS models' performance is the best when the MAD criterion is considered. The HA-ANFIS is the best model among others at GT8194049 with reference to the RMSE, R^2, and NS criteria, while the PSO-ANFIS can be treated as the top-performing model in terms of the MAE and IOA criteria. On the other hand, the DE-ANFIS is deemed to be superior when the MAD criterion is considered. It is noted that the differences in numeric values among various performance evaluation indexes are often very small. Nevertheless, decision making in this situation is very difficult if not impossible. Decision-making can be facilitated either by selecting a prediction model to be the best one when most of the performance evaluation indexes are better for that particular model or by incorporating different performance evaluation indexes. The later approach is promising because it incorporates various performance indexes to decide on the best performing model. This is often performed by assigning weights to individual models and ranking them according to the numeric values of the weights. The present study employs a MOGA for this purpose by utilizing R^2, IOA, and NS as the benefit indexes and RMSE, MAE, and MAD as the cost indexes. The outcomes are shown in Table 7. The weights presented in Table 7 are assigned to the respective prediction models to develop the ensemble model.

Table 7. Weights of the individual prediction models calculated using a Multiple Objective Genetic Algorithm at the observation wells.

Models	Weights		
	GT8194046	GT8194048	GT8194049
DE-ANFIS	0.827	0.345	0.191
PSO-ANFIS	0.157	0.133	0.112
HA-ANFIS	0.017	0.524	0.697
Sum of weights	1	1	1

3.2. Ensemble Prediction

In this section, the outcomes are presented to show the usefulness of employing an ensemble of the developed models to predict one-week ahead groundwater levels. For this purpose, a weighted-average ensemble of three prediction models is proposed in which the weights computed by the MOGA are employed to provide the ensemble prediction. The performance of the weighted average ensemble is compared with that of the individual models (DE-ANFIS, PSO-ANFIS, and HA-ANFIS) at each observation well. The comparison results are given in Table 8.

Table 8. Performance evaluation indexes of the ensemble at different observation wells.

PEI	GT8194046				GT8194048				GT8194049			
	En	DE-ANFIS	PSO-ANFIS	HA-ANFIS	En	DE-ANFIS	PSO-ANFIS	HA-ANFIS	En	DE-ANFIS	PSO-ANFIS	HA-ANFIS
RMSE	0.482	0.488	0.533	0.509	0.714	0.761	0.897	0.676	0.453	0.503	0.485	0.458
rRMSE, %	3.721	3.800	4.100	3.900	4.700	5.000	5.900	4.500	3.717	4.100	3.900	3.800
R^2	0.976	0.976	0.976	0.977	0.954	0.950	0.953	0.955	0.982	0.981	0.981	0.982
MAE	6.083	6.148	5.675	5.736	11.027	12.072	12.178	11.966	5.958	6.323	5.794	5.861
MAD	0.043	0.045	0.130	0.112	0.103	0.105	0.275	0.155	0.049	0.081	0.066	0.062
IOA	0.994	0.994	0.992	0.993	0.954	0.985	0.981	0.988	0.995	0.995	0.995	0.995
NS	0.994	0.976	0.971	0.973	0.948	0.940	0.917	0.953	0.982	0.978	0.979	0.981
a-10 index	0.980	0.980	0.985	0.984	0.980	0.978	0.973	0.979	0.980	0.981	0.981	0.981
U	0.018	0.018	0.020	0.019	0.023	0.024	0.028	0.022	0.018	0.020	0.019	0.018
U^B	0.0002	0.004	0.119	0.063	0.082	0.099	0.284	0.015	0.003	0.105	0.102	0.025
U^V	0.001	0.001	0.112	0.106	0.013	0.012	0.085	0.003	0.005	0.025	0.015	0.018
U^C	0.998	0.995	0.769	0.831	0.905	0.888	0.631	0.982	0.992	0.870	0.883	0.957
MBE	0.007	0.031	−0.184	−0.128	0.205	0.241	0.478	0.083	−0.025	0.163	−0.155	−0.072
T_{stat}	0.471	1.971	11.521	8.143	9.396	10.473	19.772	3.862	1.711	10.754	10.585	5.029
U_{95}	6.166	6.197	6.031	6.034	6.356	6.380	6.632	6.292	6.609	6.731	6.591	6.582
GPI	0.0002	0.004	−0.162	−0.074	0.398	0.622	2.667	0.061	−0.002	0.112	−0.098	−0.020

En = Ensemble.

It can be perceived from the results exhibited in Table 8 that the weighted average ensemble achieves a performance that is superior to the worst model at all instances and that the ensemble's performance is superior to the best individual model for most of the computed performance evaluation indexes. For instance, the MAD values of the ensemble at all observation wells are lower than those of the individual models indicating that the ensemble prediction for this instance is better than any individual model. On the other hand, MAE values at the observation wells GT8194046 and GT8194049 are lower than the DE-ANFIS but higher than both the PSO-ANFIS and HA-ANFIS. This indicates a better and worse performance of the ensemble compared to individual prediction models at these observation wells based on the MAE criterion. However, the MAD criterion indicates a better performance of the ensemble model over the individual models at observation well GT8194049. Decision-making in these situations is quite difficult. In such situations, if it is known a priori that a given model performs the best for a particular dataset or problem, it may be the best option to employ this model for the prediction. However, it may be difficult to recognize the top-ranked single prediction model for most problems. In this situation, an ensemble of prediction models (preferably a weighted average ensemble) may be proved to be useful in obtaining a robust and accurate prediction result.

It is observed from Table 8 that when the errors produced by all the prediction models are close to each other, as is the case of RMSE, rRMSE, R^2, MAE, IOA, and NS, for example, the prediction results of the weighted average ensemble are more accurate (smaller numeric values of RMSE, rRMSE, MAE and higher values of R^2, IOA, and NS) than any of the individual prediction models. However, when few of the models are much more imprecise than the others, the performance of the weighted average ensemble is only as accurate as of the top-performing model within the ensemble (usually, the predictions are adequately precise to those of the top prediction model). This is especially apparent in the case of MAE values at the observation well GT8194046 (Table 8). Additionally, Table 8 shows that the prediction errors of a weighted average ensemble are significantly lower than those of the worst prediction model, implying that an ensemble approach can avoid the issues

associated with picking a wrong individual model for a given situation. The findings of this study are consistent with those of [46], who proved the potential benefit of an ensemble approach on a variety of test problems of varying complexity and dimensions.

The absolute errors between actual and predicted groundwater levels produced by each individual and the ensemble models are presented in box and violin plots (Figure 10). Boxplots provide a comparative evaluation for the statistical distributions of the absolute errors of the one-week ahead groundwater levels and aids in measuring the level of overall spread of the errors made by each prediction model. The horizontal lines in each of the boxplots designate the median of the absolute errors of prediction, while the black circles mark the mean (average) of the absolute errors. The error boxplots in Figure 10 demonstrate the superiority of the ensemble and DE-ANFIS models at the observation well GT8194046, whereas HA-ANFIS appears to be the best model at GT8194048. Absolute errors produced by the DE-ANFIS, HA-ANFIS, and PSO-ANFIS are almost the same at the observation well GT8194049. Based on the error box plot, the ensemble appears to be the best performing mode at GT8194049. Figure 10 also shows the corresponding violin plots that incorporate a box plot with a kernel density plot (the kernel density plot shows the peaks in the error data). The white dot represents the median of the absolute error, the thick grey bar in the centre of a violin plot is the interquartile range, and the thin grey line denotes the rest of the distribution. The coloured region on both sides of the grey line represents the kernel density estimation for illustrating the distribution shaper of the absolute error. A higher probability is represented by the wider sections of the violin plot, while the lower probability is signified by the thinner sections (Figure 10).

The performance evaluation comparison for the ensemble and the individual prediction models is executed by ranking the models through a decision theory, Shannon's entropy. This decision theory is applied by utilizing the computed R^2, IOA, NS, RMSE, MAE, and MAD values on the test dataset by ensemble and the individual prediction models (previously calculated). The computed R^2, IOA, and NS values serve as the benefit indexes, while the RMSE, MAE, and MAD values are cost indexes. The ranking scheme for Shannon's entropy is associated with two major phases: first, the weights for the selected performance indexes are calculated, and then these weights are translated into the weights of models through the use of ideal values of the performance indexes.
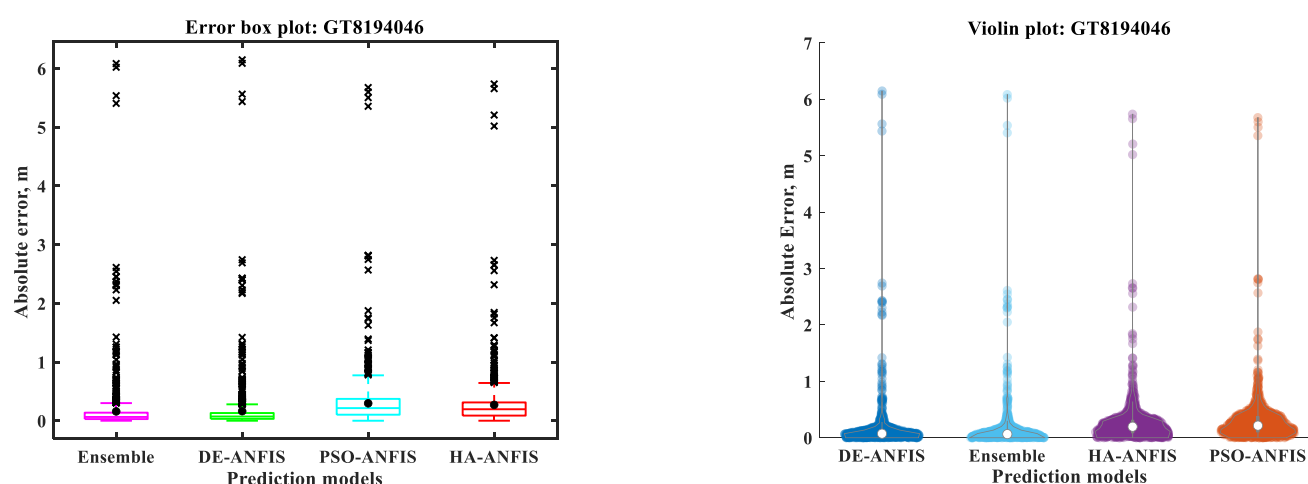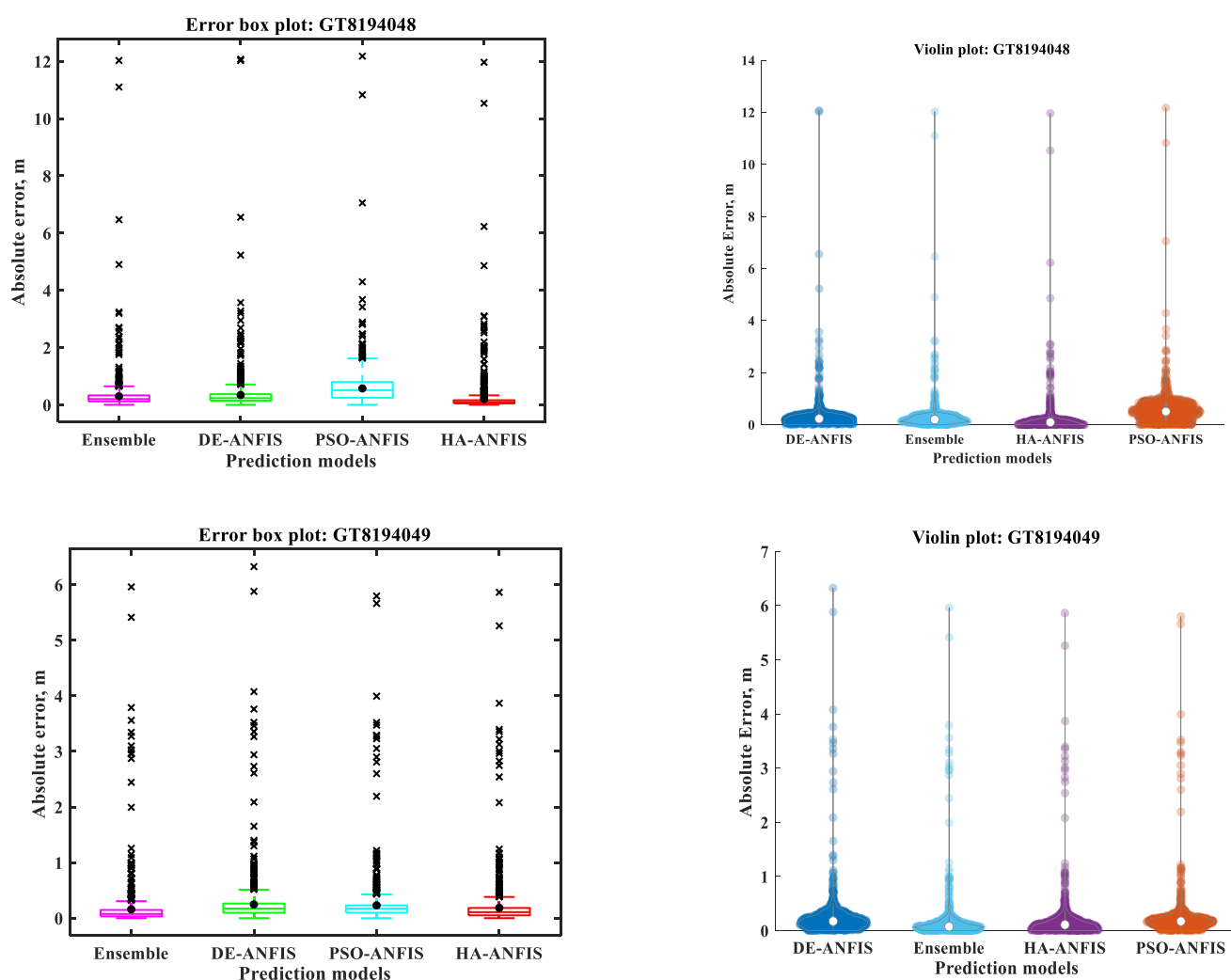

Figure 10. *Cont.*

Figure 10. Box and violin plots of the absolute errors on test dataset at the observation wells GT8194046, GT8194048, and GT8194049.

The ranking results are shown in Table 9. It is perceived from Table 9 that the weighted average ensemble receives the highest entropy weight, i.e., the ensemble prediction is better than any of the individual prediction models. Therefore, it is demonstrated that the proposed weighted average ensemble with the MOGA-based weight assignment scheme produces improved prediction results when weighed against the DE-ANFIS, PSO-ANFIS, and HA-ANFIS models' prediction outcomes. Therefore, the proposed MOGA-based weighting tactic has the potential applicability in developing the ensemble models to predict one-week ahead groundwater levels.

Table 9. Ranking of the individual and ensemble prediction models using entropy weight-based decision theory at the observation wells.

GT8194046			GT8194048			GT8194049		
Ranks	Models	Ranking Value	Ranks	Models	Ranking Value	Ranks	Models	Ranking Value
1	Ensemble	0.989	1	Ensemble	0.985	1	Ensemble	0.995
2	DE-ANFIS	0.975	2	DE-ANFIS	0.960	2	HA-ANFIS	0.959
3	HA-ANFIS	0.862	3	HA-ANFIS	0.924	3	PSO-ANFIS	0.943
4	PSO-ANFIS	0.845	4	PSO-ANFIS	0.819	4	DE-ANFIS	0.900

Overall, the study's findings confirmed that although the ensemble model is suggested due to its better performance, the DE-ANFIS, HA-ANFIS, and PSO-ANFIS can also be successfully employed to predict one-week-ahead groundwater levels. If the emphasis is placed on the high level of prediction accuracy and the reduced prediction uncertainty, then the ensemble model undoubtedly is the best choice to be implemented. As far as the individual prediction models are concerned, depending on whether the importance is given to high precision or on computational efficiency but not as much of precision, the DE-ANFIS or the HA-ANFIS models may be employed, respectively. The results obtained in this effort are entirely based on the groundwater flow lags (at a given week and the lagged periods) as inputs and the one-week ahead groundwater flow signals as outputs. The input selection is facilitated by a careful analysis of the PACF functions followed by the FLR approach of useful variable selection. Although long-term forecasting may be preferable in many water resources management problems, a short-term prediction (one-week-ahead) is adopted in the present study because of the inherent uncertainties associated with the long-term predictions with only the historical groundwater level signals.

Depleting groundwater levels have been a pressing concern in the drought-prone north-western parts of Bangladesh due to the overexploitation of the groundwater resources to meet the demands for agricultural, domestic, and industrial requirements. In the Tanore Upazila of Rajshahi district, excessive groundwater abstraction has reduced the groundwater level to a considerable amount in recent years. Therefore, the development of a precise and robust prediction tool using an ensemble of prediction models for the groundwater level fluctuations in this region can help develop a sustainable regional groundwater management strategy. Nevertheless, enhanced precision in the one-step-ahead prediction of groundwater level signals is one of the most vital aspects of developing such a robust regional or global groundwater management policy. The results obtained in this research using a weighted average ensemble of various promising machine-learning algorithms may be of great interest to the stakeholders and policymakers.

4. Performance Comparison of the Prediction Models for Forecasting 2-, 4-, 6-, and 8-Week Ahead Groundwater Level Fluctuations

The generalization capability of the proposed models and their ensemble is further investigated by employing the models to forecast groundwater levels for higher forecasting horizons (2-, 4-, 6-, and 8-week ahead). For this purpose, the generalization capability of the developed models at higher forecasting horizons is analysed for observation well GT8134046 as an example. Six statistical performance measures including benefit (R, IOA, NS, a-10 index) and cost indices (rRMSE, MAD) are calculated using actual and model-predicted groundwater level values for providing 2-, 4-, 6-, and 8-week ahead forecasting. The results are presented in Figures 11 and 12. Figure 11 presents a comparison of the performances of the individual and ensemble models based on R, IOA, NS, and a-20 index criteria. It is observed from Figure 11 that performances of the individual models do not vary substantially among the forecasting horizons indicating reliable performances of the proposed models at higher forecasting horizons. Although performances slightly deteriorate at the higher forecasting horizons, all benefit indices have values higher than 0.8 for all prediction horizons, which clearly demonstrate the acceptable performances of the models with higher accuracy even at 8-weeks ahead forecasting. It is also evident from Figure 11 that the proposed ensemble model shows superior performances for all instances of performance indices and forecasting horizons. It is worthwhile to mention that the analysis presented here is based on the data obtained from observation well GT 8134046 for demonstrating the generalization capability of the proposed ensemble modelling approach. Based on this analysis, it is perceivable that the proposed model would provide reliable performances for higher forecasting horizons at other observation wells.
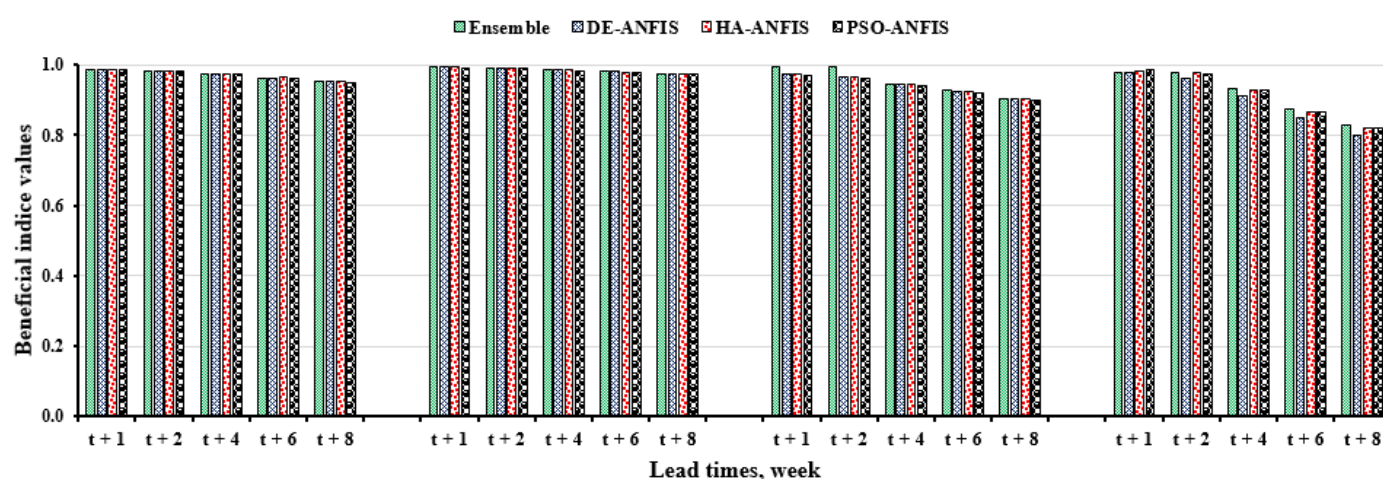
Figure 11. Performance comparison of the individual and ensemble models for forecasting the 1-, 2-, 4-, 6-, and 8-week ahead groundwater level fluctuations at GT8134046.
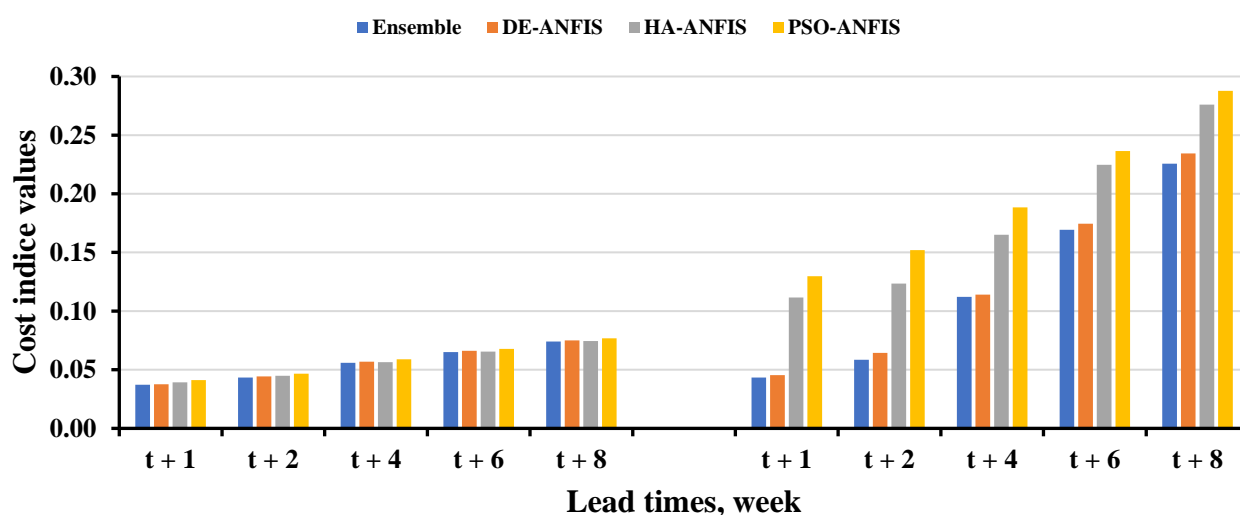

Figure 12. Performance comparison of the individual and ensemble models based on NRMSE and MAD criterion.

Performances of the models are also evaluated using NRMSE and MAD criteria. Lower values of rRMSE and MAD at all considered forecasting horizons demonstrate that the proposed models are able to forecast groundwater level values when higher forecasting horizons, e.g., 8-weeks ahead (2 months ahead) are used. Furthermore, the ensemble model produces lower values of rRMSE and MAD than the individual models, which indicates the superior performance of the ensemble model over the standalone models.

Finally, ranking of the individual and ensemble models for 2-, 4-, 6-, and 8-weeks ahead groundwater level forecasting is performed, and is presented in Table 10. It can be perceived from Table 10 that the proposed ensemble model appeared to be the top-ranked model for all considered forecast horizons. Therefore, the proposed ensemble model can be applied to forecast groundwater levels at higher forecasting horizons.

Table 10. Ranking of models using entropy weight-based decision theory for 2-, 4-, 6-, and 8-week ahead groundwater level forecasting at the observation well GT8194046.

Models	2-Week Ahead		4-Week Ahead		6-Week Ahead		8-Week Ahead	
	Ranking Value	Ranks	Ranking Value	Ranks	Ranking Value	Ranks	Ranking Value	Ranks
Ensemble	0.993	1	0.995	1	0.973	1	0.995	1
DE-ANFIS	0.962	2	0.979	2	0.911	3	0.978	2
HA-ANFIS	0.887	3	0.940	3	0.964	2	0.966	3
PSO-ANFIS	0.865	4	0.919	4	0.881	4	0.956	4

5. Conclusions

Precise and robust prediction of groundwater levels can be effectively employed in providing a short- and medium-term prediction modelling approach for groundwater level fluctuations. This study provides a robust prediction tool for one- and multi-week ahead groundwater level fluctuations through a weighted average ensemble of three optimization algorithm tuned ANFIS models (DE-ANFIS, PSO-ANFIS, and HA-ANFIS). The suitable weekly lag times of groundwater levels are used as inputs to the prediction models, while the output from the models is the one- and multi-week ahead groundwater levels. The optimal combination of inputs for the models is executed by carefully examining the PACF functions followed by performing the FLR approach. The performance comparison of the proposed models is performed by adopting a set of performance evaluation indexes. Results demonstrate that the optimized ANFIS models have sufficiently accurate predictions as indicated by the higher values of R^2, IOA, and NS as well as lower values of RMSE, MAE, and MAD. A weighted average ensemble of the optimized ANFIS models is proposed to achieve more reliable and accurate predictions. The weights of the individual prediction models computed by a Multiple Objective Genetic Algorithm (MOGA) are used to construct the ensemble of the optimized ANFIS models. The performance evaluation indexes for the ensemble prediction are computed and compared with those of the individual models. The performance comparison is performed using a ranking scheme of a well-known decision theory, Shannon's entropy. The results of this ranking scheme reveal the superiority of the ensemble models over all the individual models.

The most important finding of this study is that employing a weighted-average ensemble of data-driven prediction models can improve predictions' robustness by minimizing the influence of a worse-performing prediction model. This is especially important because it is difficult, if not impossible, to select the best prediction model for a particular problem due to a vast number of alternatives and that the best prediction model can be changed with the changes in the dataset. Therefore, it can be concluded that the proposed weighted average ensemble approach can be considered as a robust approximation method for predicting one-week-ahead groundwater level fluctuations for the selected observation wells. Furthermore, groundwater level forecasts conducted for 2-, 4-, 6-, and 8-weeks in advance using data from the observation well GT8194046 reveal the potential applicability of the ensemble approach proposed in this effort. Future research may be directed towards applying the proposed approach in predicting multi-step-ahead groundwater level fluctuations at other locations.

Appendix A

Appendix A.1. Performance Evaluation Indexes

The performance evaluation indexes employed to evaluate the performance of all standalone optimized ANFIS models, as well as their ensemble, are given below.

Correlation Coefficient, *R*

$$R = \frac{\sum_{i=1}^{n}\left(GL_{i,a} - \overline{GL_a}\right)\left(GL_{i,a} - \overline{GL_p}\right)}{\sqrt{\sum_{i=1}^{n}\left(GL_{i,a} - \overline{GL_a}\right)^2}\sqrt{\sum_{i=1}^{n}\left(GL_{i,p} - \overline{GL_p}\right)^2}} \tag{A1}$$

Relative RMSE, rRMSE

$$rRMSE = \frac{RMSE}{\overline{GL_a}} = \frac{\sqrt{\frac{1}{n}\sum_{i=1}^{n}\left(GL_{i,a} - GL_{i,p}\right)^2}}{\overline{GL_a}} \tag{A2}$$

The rRMSE is often referred to as the Scatter Index (*SI*), which provides a qualitative comparison of model performances (excellent, good, fair, and poor). The *SI* index classifies a model as acceptable or unacceptable according to the following criteria

$$\begin{array}{c} SI < 0.1 \ Excellent \\ 0.1 < SI < 0.2 \ Good \\ 0.2 < SI < 0.3 \ Fair \\ SI > 0.3 \ Poor \end{array} \tag{A3}$$

Maximum Absolute Error, *MAE*

$$MAE = max\left[\left|GL_{i,a} - GL_{i,p}\right|\right] \tag{A4}$$

Median Absolute Deviation, *MAD*

$$MAD\left(GL_a, GL_p\right) = median\left(\left|GL_{1,a} - GL_{1,p}\right|, \left|GL_{2,a} - GL_{2,p}\right|, \ldots, \left|GL_{n,a} - GL_{n,p}\right|\right)$$
$$for \ i = 1, 2, \ldots, n \tag{A5}$$

Mean Bias Error, *MBE*

$$MBE = \frac{1}{n}\sum_{i=1}^{n}\left(GL_{i,a} - GL_{i,p}\right) \tag{A6}$$

T-statistic test, T_{stat} [91]

$$T_{stat} = \sqrt{\frac{(n-1) * MBE^2}{RMSE^2 - MBE^2}} \tag{A7}$$

Uncertainty with 95% confidence level, U_{95}

$$U_{95} = 1.96 \times \sqrt{Standard \ deviation^2 - RMSE^2} \tag{A8}$$

Global Performance Index, *GPI*

$$GPI = MBE * RMSE * U_{95} * T_{stat} * \left(1 - R^2\right) \tag{A9}$$

Nash–Sutcliffe Efficiency Coefficient, *NS*

$$NS = 1 - \frac{\sum_{i=1}^{n}\left(GL_{i,a} - GL_{i,p}\right)^2}{\sum_{i=1}^{n}\left(GL_{i,a} - \overline{GL_a}\right)^2} \tag{A10}$$

Theil inequality statistics, U

$$U = \frac{\sqrt{\frac{1}{n}\sum(GL_{i,p} - GL_{i,a})^2}}{\sqrt{\frac{1}{n}\sum(GL_{i,p})^2} + \sqrt{\frac{1}{n}\sum(GL_{i,a})^2}} \tag{A11}$$

Bias proportion of Theil inequality statistics, U^B

$$U^B = \frac{\left(\overline{GL_p} - \overline{GL_a}\right)^2}{(1/T)\sum(GL_{i,p} - GL_{i,a})^2} \tag{A12}$$

Variance proportion of Theil inequality statistics, U^V

$$U^V = \frac{\left(\sigma_p - \sigma_a\right)^2}{(1/T)\sum(GL_{i,p} - GL_{i,a})^2} \tag{A13}$$

Covariance proportion of Theil inequality statistics, U^C

$$U^C = \frac{2(1 - R)\sigma_p\sigma_a}{(1/T)\sum(GL_{i,p} - GL_{i,a})^2} \tag{A14}$$

where $GL_{i,a}$ and $GL_{i,p}$ represent actual (obtained) and model predicted GL values at the ith step, respectively; $\overline{GL_a}$ is the mean value of the actual GL values; σ_a indicates standard deviation value of the actual GL, σ_p denotes standard deviation of the predicted GL values, n represents the numeral of data points, ED is the Euclidian distance of any data points from their ideal values, $\propto$ is relative variability in the predicted and actual GL values, and β is the ratio between the mean (average) predicted and mean (average) actual GL data demonstrating the bias.

In addition, according to a recently proposed engineering index, $a^{20} - index$, we calculated an $a^{10} - index$ to assess the reliability of the developed prediction models.

$$a^{10} - index = \frac{m^{10}}{M} \tag{A15}$$

where, M denotes the quantity of test datasets and m^{10} is the numeral of test samples that have a *Actual value/Predicted value* ranging between 0.90–1.10. For an impeccable data-driven prediction modelling approach, the numeric value of $a^{10} - index$ is anticipated to have a value of unity (i.e., 1). The values of $a^{10} - index$ has physical engineering significance: it states that the number of samples that comply with forecasted values within a range of variation of $\pm 10\%$ weighed against the actual values.

Appendix A.2. Ranking of the Prediction Models Using Shannon's Entropy

The following steps are used to calculate Shannon's entropy:

Step 1: Formation of a decision matrix of prediction models (individual models and the ensemble) and performance evaluation indexes. It is assumed that there be m prediction models and n performance evaluation indexes. Then, the resulting decision matrix is given by:

$$GL_{ij} = \begin{bmatrix} GL_{11} & GL_{21} & \cdots & GL_{m1} \\ GL_{12} & GL_{22} & \cdots & GL_{m2} \\ \vdots & \vdots & \vdots & \vdots \\ GL_{1n} & GL_{2n} & \cdots & GL_{mn} \end{bmatrix} \tag{A16}$$

Step 2: Standardization of the decision matrix for minimizing the impacts of index dimensionality. The performance index values are standardized between 0–1 ($S_{ij} \in [0,1]$, $i = 1, 2, \ldots, m; j = 1, 2, \ldots, n$). The values of S_{ij} are computed as:

$$S_{ij} = \begin{cases} \frac{GL_{ij}}{max(GL_{i1}, GL_{i2}, \ldots, GL_{in})}, & for\ benefit\ indexes \\ \frac{GL_{ij}}{min(GL_{i1}, GL_{i2}, \ldots, GL_{in})}, & for\ cost\ indexes \end{cases} \tag{A17}$$

Step 3: Computation of each index's *entropy* via utilizing the concepts of Shannon's *entropy*. The *entropy* value of the *j*th index was calculated as:

$$Entropy_j = -k \sum_{i=1}^{m} f_{ij} ln f_{ij} \tag{A18}$$

where,

$$f_{ij} = S_{ij} / \sum_{i=1}^{m} S_{ij} \tag{A19}$$

$$k = 1/lnm \tag{A20}$$

Step 4: Calculation of each index's *entropy* weight value. The *j*th index's *entropy* weight was calculated as:

$$w(entropy)_j = \frac{1 - Entropy_j}{n - \sum_{j=1}^{n} Entropy_j} \tag{A21}$$

This *entropy*-based weight designates the prominence of any particular performance index in the phases of the entire decision-making. The larger the numeric value of the *entropy* weight, the greater information the specific index conveys, and the more significant this performance index will become in the decision-making process.

Step 5: Calculation of each model's rank weight is carried out by summing up the multiplication of every index's *entropy* weight and the normalized value of that particular index. This step is mathematically represented by:

$$w(entropy)_i = \sum_{j=1}^{n} S_{ij} \times w(entropy)_j \tag{A22}$$

Step 6: Determination of model ranking

$$max\ [w(entropy)_i], \ldots, min[w(entropy)_i]; for\ i = 1, 2, \ldots, m \tag{A23}$$

References

1. Wada, Y.; Bierkens, M.F.P. Sustainability of global water use: Past reconstruction and future projections. *Environ. Res. Lett.* **2014**, *9*, 104003. [CrossRef]
2. Hoque, M.A.; Adhikary, S.K. Prediction of groundwater level using artificial neural network and multivariate time series models. In Proceedings of the 5th International Conference on Civil Engineering and Sustainable Development (ICCESD 2020), Khulna, Bangladesh, 7–9 February 2020; pp. 1–8.
3. Doble, R.C.; Pickett, T.; Crosbie, R.S.; Morgan, L.K.; Turnadge, C.; Davies, P.J. Emulation of recharge and evapotranspiration processes in shallow groundwater systems. *J. Hydrol.* **2017**, *555*, 894–908. [CrossRef]
4. Masterson, J.P.; Garabedian, S.P. Effects of sea-level rise on ground water flow in a coastal aquifer system. *Groundwater* **2007**, *45*, 209–217. [CrossRef] [PubMed]
5. Park, E.; Parker, J.C. A simple model for water table fluctuations in response to precipitation. *J. Hydrol.* **2008**, *356*, 344–349. [CrossRef]
6. Fahimi, F.; Yaseen, Z.M.; El-shafie, A. Application of soft computing based hybrid models in hydrological variables modeling: A comprehensive review. *Theor. Appl. Climatol.* **2017**, *128*, 875–903. [CrossRef]
7. Govindaraju, R.S. Artificial neural networks in hydrology. I: Preliminary concepts. *J. Hydrol. Eng.* **2000**, *5*, 115–123. [CrossRef]
8. Govindaraju, R.S. Artificial neural networks in hydrology. II: Hydrologic applications. *J. Hydrol. Eng.* **2000**, *5*, 124–137.
9. Maier, H.R.; Jain, A.; Dandy, G.C.; Sudheer, K.P. Methods used for the development of neural networks for the prediction of water resource variables in river systems: Current status and future directions. *Environ. Model. Softw.* **2010**, *25*, 891–909. [CrossRef]

10. Sadler, J.M.; Goodall, J.L.; Morsy, M.M.; Spencer, K. Modeling urban coastal flood severity from crowd-sourced flood reports using Poisson regression and Random Forest. *J. Hydrol.* **2018**, *559*, 43–55. [CrossRef]

11. Yang, T.; Asanjan, A.A.; Welles, E.; Gao, X.; Sorooshian, S.; Liu, X. Developing reservoir monthly inflow forecasts using artificial intelligence and climate phenomenon information. *Water Resour. Res.* **2017**, *53*, 2786–2812. [CrossRef]

12. Yaseen, Z.M.; El-shafie, A.; Jaafar, O.; Afan, H.A.; Sayl, K.N. Artificial intelligence based models for stream-flow forecasting: 2000–2015. *J. Hydrol.* **2015**, *530*, 829–844. [CrossRef]

13. Solomatine, D.P.; Ostfeld, A. Data-driven modelling: Some past experiences and new approaches. *J. Hydroinform.* **2008**, *10*, 3–22. [CrossRef]

14. Karandish, F.; Šimůnek, J. A comparison of numerical and machine-learning modeling of soil water content with limited input data. *J. Hydrol.* **2016**, *543*, 892–909. [CrossRef]

15. Mohanty, S.; Jha, M.K.; Kumar, A.; Panda, D.K. Comparative evaluation of numerical model and artificial neural network for simulating groundwater flow in Kathajodi–Surua Inter-basin of Odisha, India. *J. Hydrol.* **2013**, *495*, 38–51. [CrossRef]

16. Adamowski, J.; Chan, H.F. A wavelet neural network conjunction model for groundwater level forecasting. *J. Hydrol.* **2011**, *407*, 28–40. [CrossRef]

17. Daliakopoulos, I.N.; Coulibaly, P.; Tsanis, I.K. Groundwater level forecasting using artificial neural networks. *J. Hydrol.* **2005**, *309*, 229–240. [CrossRef]

18. Obergfell, C.; Bakker, M.; Maas, K. Identification and explanation of a change in the groundwater regime using time series analysis. *Groundwater* **2019**, *57*, 886–894. [CrossRef]

19. Roshni, T.; Jha, M.K.; Deo, R.C.; Vandana, A. Development and evaluation of hybrid artificial neural network architectures for modeling spatio-temporal groundwater fluctuations in a complex aquifer system. *Water Resour. Manag.* **2019**, *33*, 2381–2397. [CrossRef]

20. Feng, S.; Kang, S.; Huo, Z.; Chen, S.; Mao, X. Neural networks to simulate regional ground water levels affected by human activities. *Groundwater* **2008**, *46*, 80–90. [CrossRef]

21. Guzman, S.M.; Paz, J.O.; Tagert, M.L.M. The use of NARX neural networks to forecast daily groundwater levels. *Water Resour. Manag.* **2017**, *31*, 1591–1603. [CrossRef]

22. Sahoo, S.; Russo, T.A.; Elliott, J.; Foster, I. Machine learning algorithms for modeling groundwater level changes in agricultural regions of the U.S. *Water Resour. Res.* **2017**, *53*, 3878–3895. [CrossRef]

23. Zhang, Z.; Zhang, Q.; Singh, V.P. Univariate streamflow forecasting using commonly used data-driven models: Literature review and case study. *Hydrol. Sci. J.* **2018**, *63*, 1091–1111. [CrossRef]

24. Dong, L.; Guangxuan, L.; Qiang, F.; Mo, L.; Chunlei, L.; Abrar, F.M.; Imran, K.M.; Tianxiao, L.; Song, C. Application of particle swarm optimization and extreme learning machine forecasting models for regional groundwater depth using nonlinear prediction models as preprocessor. *J. Hydrol. Eng.* **2018**, *23*, 4018052.

25. Mohanty, S.; Jha, M.K.; Raul, S.K.; Panda, R.K.; Sudheer, K.P. Using artificial neural network approach for simultaneous forecasting of weekly groundwater levels at multiple sites. *Water Resour. Manag.* **2015**, *29*, 5521–5532. [CrossRef]

26. Ghorbani, M.A.; Deo, R.C.; Karimi, V.; Yaseen, Z.M.; Terzi, O. Implementation of a hybrid MLP-FFA model for water level prediction of Lake Egirdir, Turkey. *Stoch. Environ. Res. Risk Assess.* **2018**, *32*, 1683–1697. [CrossRef]

27. Lee, S.; Lee, K.-K.; Yoon, H. Using artificial neural network models for groundwater level forecasting and assessment of the relative impacts of influencing factors. *Hydrogeol. J.* **2019**, *27*, 567–579. [CrossRef]

28. Barzegar, R.; Fijani, E.; Asghari Moghaddam, A.; Tziritis, E. Forecasting of groundwater level fluctuations using ensemble hybrid multi-wavelet neural network-based models. *Sci. Total Environ.* **2017**, *599–600*, 20–31. [CrossRef]

29. Peng, T.; Zhou, J.; Zhang, C.; Fu, W. Streamflow forecasting using empirical wavelet transform and artificial neural networks. *Water* **2017**, *9*, 406. [CrossRef]

30. Raghavendra, S.N.; Deka, P.C. Forecasting monthly groundwater level fluctuations in coastal aquifers using hybrid Wavelet packet–Support vector regression. *Cogent Eng.* **2015**, *2*, 999414. [CrossRef]

31. Gong, Y.; Wang, Z.; Xu, G.; Zhang, Z. A comparative study of groundwater level forecasting using data-driven models based on ensemble empirical mode decomposition. *Water* **2018**, *10*, 730. [CrossRef]

32. Boubaker, S. Identification of monthly municipal water demand system based on autoregressive integrated moving average model tuned by particle swarm optimization. *J. Hydroinform.* **2017**, *19*, 261–281. [CrossRef]

33. Banadkooki, F.B.; Ehteram, M.; Ahmed, A.N.; Teo, F.Y.; Fai, C.M.; Afan, H.A.; Sapitang, M.; El-Shafie, A. Enhancement of groundwater-level prediction using an integrated machine learning model optimized by whale algorithm. *Nat. Resour. Res.* **2020**, *29*, 3233–3252. [CrossRef]

34. Makungo, R.; Odiyo, J.O. Estimating groundwater levels using system identification models in Nzhelele and Luvuvhu areas, Limpopo Province, South Africa. *Phys. Chem. Earth* **2017**, *100*, 44–50. [CrossRef]

35. Nadiri, A.A.; Naderi, K.; Khatibi, R.; Gharekhani, M. Modelling groundwater level variations by learning from multiple models using fuzzy logic. *Hydrol. Sci. J.* **2019**, *64*, 210–226. [CrossRef]

36. Nourani, V.; Mousavi, S. Spatiotemporal groundwater level modeling using hybrid artificial intelligence-meshless method. *J. Hydrol.* **2016**, *536*, 10–25. [CrossRef]

37. Wen, X.; Feng, Q.; Yu, H.; Wu, J.; Si, J.; Chang, Z.; Xi, H. Wavelet and adaptive neuro-fuzzy inference system conjunction model for groundwater level predicting in a coastal aquifer. *Neural Comput. Appl.* **2015**, *26*, 1203–1215. [CrossRef]

38. Zare, M.; Koch, M. Groundwater level fluctuations simulation and prediction by ANFIS- and hybrid Wavelet-ANFIS/Fuzzy C-Means (FCM) clustering models: Application to the Miandarband plain. *J. Hydro-Environ. Res.* **2018**, *18*, 63–76. [CrossRef]
39. Moosavi, V.; Vafakhah, M.; Shirmohammadi, B.; Behnia, N. A wavelet-ANFIS hybrid model for groundwater level forecasting for different prediction periods. *Water Resour. Manag.* **2013**, *27*, 1301–1321. [CrossRef]
40. Tang, Y.; Zang, C.; Wei, Y.; Jiang, M. Data-driven modeling of groundwater level with least-square support vector machine and spatial–temporal analysis. *Geotech. Geol. Eng.* **2019**, *37*, 1661–1670. [CrossRef]
41. Wei, Z.-L.; Wang, D.-F.; Sun, H.-Y.; Yan, X. Comparison of a physical model and phenomenological model to forecast groundwater levels in a rainfall-induced deep-seated landslide. *J. Hydrol.* **2020**, *586*, 124894. [CrossRef]
42. Fallah-Mehdipour, E.; Bozorg Haddad, O.; Mariño, M.A. Prediction and simulation of monthly groundwater levels by genetic programming. *J. Hydro-Environ. Res.* **2013**, *7*, 253–260. [CrossRef]
43. Aguilera, H.; Guardiola-Albert, C.; Naranjo-Fernández, N.; Kohfahl, C. Towards flexible groundwater-level prediction for adaptive water management: Using Facebook's Prophet forecasting approach. *Hydrol. Sci. J.* **2019**, *64*, 1504–1518. [CrossRef]
44. Ghaseminejad, A.; Uddameri, V. Physics-inspired integrated space-time artificial neural networks for regional groundwater flow modeling. *Hydrol. Earth Syst. Sci.* **2020**, *24*, 5759–5779. [CrossRef]
45. Rajaee, T.; Ebrahimi, H.; Nourani, V. A review of the artificial intelligence methods in groundwater level modeling. *J. Hydrol.* **2019**, *572*, 336–351. [CrossRef]
46. Goel, T.; Haftka, R.T.; Shyy, W.; Queipo, N.V. Ensemble of surrogates, Struct. *Multidiscip. Optim.* **2007**, *33*, 199–216. [CrossRef]
47. Jafari, S.A.; Mashohor, S.; Varnamkhasti, M.J. Committee neural networks with fuzzy genetic algorithm. *J. Pet. Sci. Eng.* **2011**, *76*, 217–223. [CrossRef]
48. Roy, D.K.; Datta, B. Multivariate adaptive regression spline ensembles for management of multilayered coastal aquifers. *J. Hydrol. Eng.* **2017**, *22*, 4017031. [CrossRef]
49. Sreekanth, J.; Datta, B. Coupled simulation-optimization model for coastal aquifer management using genetic programming-based ensemble surrogate models and multiple-realization optimization. *Water Resour. Res.* **2011**, *47*. [CrossRef]
50. Zerpa, L.E.; Queipo, N.V.; Pintos, S.; Salager, J.-L. An optimization methodology of alkaline–surfactant–polymer flooding processes using field scale numerical simulation and multiple surrogates. *J. Pet. Sci. Eng.* **2005**, *47*, 197–208. [CrossRef]
51. Shannon, C.E. A mathematical theory of communication. *Bell Syst. Tech. J.* **1948**, *27*, 379–423. [CrossRef]
52. Zhao, K.Q.; Xuan, A.L. Set pair theory-a new theory method of non-define and its applications. *Syst. Eng.* **1996**, *14*, 18–23.
53. Dempster, A.P. *Upper and Lower Probabilities Induced by a Multivalued Mapping BT-Classic Works of the Dempster-Shafer Theory of Belief Functions*; Yager, R.R., Liu, L., Eds.; Springer: Berlin/Heidelberg, Germany, 2008; pp. 57–72.
54. Shafer, G. A mathematical theory of evidence turns 40. *Int. J. Approx. Reason.* **2016**, *79*, 7–25. [CrossRef]
55. Goldberg, D.E.; Holland, J.H. Genetic algorithms and machine learning. *Mach. Learn.* **1988**, *3*, 95–99. [CrossRef]
56. Shen, Z.-Q.; Kong, F.-S. *Optimizing Weights by Genetic Algorithm for Neural Network Ensemble BT-Advances in Neural Networks–ISNN 2004*; Yin, F.-L., Wang, J., Guo, C., Eds.; Springer: Berlin/Heidelberg, Germany, 2004; pp. 323–331.
57. Roy, D.K.; Datta, B. Selection of meta-models to predict saltwater intrusion in coastal aquifers using entropy weight based decision theory. In Proceedings of the 2018 IEEE Conference on Technologies for Sustainability (SusTech), Long Beach, CA, USA, 11–13 November 2018; pp. 1–6.
58. Roy, D.K.; Datta, B. An ensemble meta-modelling approach using the Dempster-Shafer theory of evidence for developing saltwater intrusion management strategies in coastal aquifers. *Water Resour. Manag.* **2019**, *33*, 775–795. [CrossRef]
59. Roy, D.K.; Datta, B. Saltwater intrusion prediction in coastal aquifers utilizing a weighted-average heterogeneous ensemble of prediction models based on Dempster-Shafer theory of evidence. *Hydrol. Sci. J.* **2020**, *65*, 1555–1567. [CrossRef]
60. Deb, K.; Pratap, A.; Agarwal, S.; Meyarivan, T. A fast and elitist multiobjective genetic algorithm: NSGA-II. *IEEE Trans. Evol. Comput.* **2002**, *6*, 182–197. [CrossRef]
61. Mohanty, S.; Jha, M.K.; Kumar, A.; Sudheer, K.P. Artificial neural network modeling for groundwater level forecasting in a river island of eastern India. *Water Resour. Manag.* **2010**, *24*, 1845–1865. [CrossRef]
62. Wang, X.; Liu, T.; Zheng, X.; Peng, H.; Xin, J.; Zhang, B. Short-term prediction of groundwater level using improved random forest regression with a combination of random features. *Appl. Water Sci.* **2018**, *8*, 1–12. [CrossRef]
63. Huang, F.; Huang, J.; Jiang, S.H.; Zhou, C. Prediction of groundwater levels using evidence of chaos and support vector machine. *J. Hydroinform.* **2017**, *19*, 586–606. [CrossRef]
64. SRDI. *Upazila Land and Soil Resource Utilization Guide: Tanore, Rajshahi*; SRDI: Dhaka, Bangladesh, 2000.
65. SRDI. *Land and Soil Statistical Appraisal Book of Bangladesh*; SRDI (Soil Resource Development Institute): Dhaka, Bangladesh, 2010.
66. Mathworks, Technical Documentation, Impute Missing Data Using Nearest-Neighbor Method. 2020. Available online: https://au.mathworks.com/help/bioinfo/ref/knnimpute.html (accessed on 23 April 2020).
67. Troyanskaya, O.; Cantor, M.; Sherlock, G.; Brown, P.; Hastie, T.; Tibshirani, R.; Botstein, D.; Altman, R.B. Missing value estimation methods for DNA microarrays. *Bioinformatics* **2001**, *17*, 520–525. [CrossRef]
68. Hastie, T.; Tibshirani, R.; Sherlock, G.; Eisen, M.; Brown, P.; Botstein, D. *Imputing Missing Data for Gene Expression Arrays*; Technical Report; Division of Biostatistics, Stanford University: Stanford, CA, USA, 1999.
69. Deo, R.C.; Tiwari, M.K.; Adamowski, J.F.; Quilty, J.M. Forecasting effective drought index using a wavelet extreme learning machine (W-ELM) model. *Stoch. Environ. Res. Risk Assess.* **2017**, *31*, 1211–1240. [CrossRef]

70. Mouatadid, S.; Adamowski, J.; Tiwari, M.K.; Quilty, J.M. Coupling the maximum overlap discrete wavelet transform and long short-term memory networks for irrigation flow forecasting. *Agric. Water Manag.* **2019**, *219*, 72–85. [CrossRef]

71. Tibshirani, R. Regression Shrinkage and Selection via the Lasso. *J. R. Stat. Soc. Ser. B* **1996**, *58*, 267–288. [CrossRef]

72. Mathworks, Technical Documentation: Zscore, Stand. z-Scores. 2020. Available online: https://au.mathworks.com/help/stats/zscore.html (accessed on 2 May 2020).

73. Jang, J.-S.R.; Sun, C.T.; Mizutani, E. *Neuro-Fuzzy and Soft Computing: A Computational Approach to Learning and Machine Intelligence*; Prentice Hall: Upper Saddle River, NJ, USA, 1997.

74. Sugeno, M.; Yasukawa, T. A fuzzy-logic-based approach to qualitative modeling. *IEEE Trans. Fuzzy Syst.* **1993**, *1*, 7. [CrossRef]

75. Takagi, T.; Sugeno, M. Fuzzy identification of systems and its applications to modeling and control. *IEEE Trans. Syst. Man. Cybern.* **1985**, *SMC-15*, 116–132. [CrossRef]

76. Bezdek, J.C.; Ehrlich, R.; Full, W. FCM: The fuzzy c-means clustering algorithm. *Comput. Geosci.* **1984**, *10*, 191–203. [CrossRef]

77. Jang, J.-S.R. ANFIS: Adaptive-network-based fuzzy inference system. *IEEE Trans. Syst. Man. Cybern.* **1993**, *23*, 665–685. [CrossRef]

78. Werbos, P.J. Beyond Regression: New Tools for Prediction and Analysis in the Behavioral Sciences. Ph.D. Dissertation, Harvard University, Cambridge, MA, USA, 1974.

79. Price, K.V. *An Introduction to Differential Evolution*; Corne, D., Dorigo, M., Glover, F., Eds.; New Ideas Optim., McGraw-Hill Ltd.: London, UK, 1999; pp. 79–108.

80. Storn, R. *Designing Digital Filters with Differential Evolution*; Corne, D., Dorigo, M., Glover, F., Eds.; New Ideas Optim., McGraw-Hill Ltd.: London, UK, 1999; pp. 109–126.

81. Storn, R.; Price, K. Differential evolution—A simple and efficient heuristic for global optimization over continuous spaces. *J. Glob. Optim.* **1997**, *11*, 341–359. [CrossRef]

82. Fan, H.-Y.; Lampinen, J. A trigonometric mutation operation to differential evolution. *J. Glob. Optim.* **2003**, *27*, 105–129. [CrossRef]

83. Das, S.; Suganthan, P.N. Differential evolution: A survey of the state-of-the-art. *IEEE Trans. Evol. Comput.* **2011**, *15*, 4–31. [CrossRef]

84. Kennedy, J.; Eberhart, R. Particle swarm optimization. In Proceedings of the ICNN'95—International Conference on Neural Networks, Perth, WA, USA, 27 November–1 December 1995; Volume 4, pp. 1942–1948.

85. Sun, L.; Song, X.; Chen, T. An improved convergence particle swarm optimization algorithm with random sampling of control parameters. *J. Control Sci. Eng.* **2019**, 7478498.

86. Deng, J.-L. Control problems of grey systems. *Syst. Control Lett.* **1982**, *1*, 288–294.

87. Wang, Z.; Rangaiah, G.P. Application and analysis of methods for selecting an optimal solution from the Pareto-optimal front obtained by multiobjective optimization. *Ind. Eng. Chem. Res.* **2017**, *56*, 560–574. [CrossRef]

88. Roy, D.K.; Datta, B. A review of surrogate models and their ensembles to develop saltwater intrusion management strategies in coastal aquifers. *Earth Syst. Environ.* **2018**, *2*, 193–211. [CrossRef]

89. Wu, J.; Sun, J.; Liang, L.; Zha, Y. Determination of weights for ultimate cross efficiency using Shannon entropy. *Expert Syst. Appl.* **2011**, *38*, 5162–5165. [CrossRef]

90. Li, X.; Wang, K.; Liu, L.; Xin, J.; Yang, H.; Gao, C. Application of the entropy weight and TOPSIS method in safety evaluation of coal mines. *Procedia Eng.* **2011**, *26*, 2085–2091. [CrossRef]

91. Stone, R.J. Improved statistical procedure for the evaluation of solar radiation estimation models. *Sol. Energy* **1993**, *51*, 289–291. [CrossRef]

92. Behar, O.; Khellaf, A.; Mohammedi, K. Comparison of solar radiation models and their validation under Algerian climate–The case of direct irradiance. *Energy Convers. Manag.* **2015**, *98*, 236–251. [CrossRef]

93. Gueymard, C.A. A review of validation methodologies and statistical performance indicators for modeled solar radiation data: Towards a better bankability of solar projects. *Renew. Sustain. Energy Rev.* **2014**, *39*, 1024–1034. [CrossRef]